Vibrational Spectroscopic Studies of Aqueous Interfaces: Salts, Acids, Bases, and Nanodrops

Sandhya Gopalakrishnan, Dingfang Liu, and Heather C. Allen*

Department of Chemistry, The Ohio State University, Columbus, Ohio 43210

Margaret Kuo and Mary Jane Shultz*

Department of Chemistry, Pearson Laboratory, Tufts University, Medford, Massachusetts 02155

Received May 27, 2005

Contents

1. Introduction 1155
2. Sum Frequency Generation 1155
   2.1. Optical Factors and Electric Fields 1157
   2.2. Nonlinear Susceptibility and Orientation 1158
   2.3. Observed Intensity—Interference 1159
      2.3.1. Spectral Fits 1159
   2.4. Experimental Section 1159
3. Results and Discussion 1159
   3.1. Spectroscopy—Spectral Assignments of Neat Water 1159
   3.2. Salts 1161
      3.2.1 Sodium Halides 1161
      3.2.2. Ammonium and Sulfate Salts 1163
      3.2.3. Sulfate and Bisulfate Salts 1164
   3.3. Acids 1165
   3.4. Acids versus Salts 1168
   3.5. Cluster Studies on Protonated Water 1169
   3.6. Ammonia 1170
   3.7. Nanodrops 1171
4. Conclusions and Summary 1173
5. Acknowledgments 1173
6. References Cited 1173

1. Introduction

The ubiquitous nature of water makes the study of water both practical and relevant. Yet in this advanced technological age, many important, fundamental questions remain unanswered about water and the aqueous interface. As we learn more about water, more questions arise. The fact that water molecules strongly hydrogen bond to one another explains, at the most basic level, the inherently high boiling point of water. Moreover, the surface structure of water, directly related to the hydrogen bonding between water molecules, is unique. It is the nature of the hydrogen bond that makes understanding water and aqueous interfaces such a challenge: hydrogen bonding is dynamic and is a strong intermolecular force, yet it is considerably weaker than a covalent bond. Due to the experimental and theoretical challenges presented by the hydrogen bond, the scientific community is far from a full understanding of bulk and surface water.

In this review, we focus on spectroscopic studies of surface water structure as it is affected by salts, acids, and ammonia. Cluster studies contribute to understanding the aqueous interface, and these are discussed along with studies of aqueous nanodrops.

2. Sum Frequency Generation

Two factors make experimentally probing an aqueous solution interface a challenge. First, the interface is inherently dynamic. For example, at 0 °C, the vapor pressure of water (∼4.5 Torr) results in exchange between the gas phase and the surface of about three million monolayers per second.[1] It is thus surprising that a spectrum of the surface contains features other than broad bands due to the ever-changing environment. Second, under most experimental conditions, the aqueous solution is in contact with the vapor phase or another condensed phase and the number densities are much larger in both a condensed and a vapor phase than on the surface. These two factors conspire to render most surface science techniques unsuitable for probing the aqueous/air interface. The optical techniques discussed in this review circumvent these two factors by selectively generating a signal only from the interface. Signal generation is based on the nonlinear polarization of the interface that results from the asymmetric environment found there. Since both the bulk aqueous solution and the gas phases are isotropic, these phases do not contribute to the observed resonances and, hence, do not interfere with detection of surface species. The appearance of resonances despite the dynamic nature of the interface indicates that the asymmetric environment results in a net polar orientation of surface molecules.

Two nonlinear techniques, second harmonic generation (SHG) and sum frequency generation (SFG), have been used to probe the aqueous interface.[1−8] The theoretical basis for these techniques was set out by Bloembergen and Pershan in the 1960s.[9] SHG and SFG differ in the resonances probed. SHG results from the combination of two visible or near-infrared photons (Figure 1) and, so, accesses the electronic states of the surface molecules. Shen and co-workers[10] pioneered application of SHG to study a liquid interface. The first report involved *p*-nitrobenzoic acid on water and illustrates a limitation of SHG for probing mixtures. The polarizability of the nitro group across the phenyl ring from the acid group results in a strongly directed molecular polarizability and hyperpolarizability. Analysis of the po-

10.1021/cr040361n CCC: $59.00
Published on Web 02/22/2006

Sandhya Gopalakrishnan received her Ph.D. in 2002 in Physical Chemistry from The Ohio State University and did postdoctoral research in the study of surfaces relevant to atmospheric aerosol chemistry using nonlinear spectroscopy. Dr. Gopalakrishnan was awarded the Rao Prize for one of the most outstanding student talks at the International Symposium of Molecular Spectroscopy in 2002 and was an invited speaker at the Atmospheric Chemistry Colloquium for Emerging Senior Scientists (ACCESS) in 2003. Dr. Gopalakrishnan is currently working at KLA-Tencor Corporation in Milpitas, California.

Dingfang Liu received a B.S. degree in Environmental Engineering (1993) at Nanchang Institute of Aeronautical Technology China, a Masters degree in Environmental Science (1999) at Chinese Academy of Science Beijing, and a Ph.D. in Civil Engineering (2002) at Louisiana State University Baton Rouge. His Masters degree advisor was Professor Zijian Wang, and his Ph.D. advisor was Professor John J. Sanslone. He worked as a postdoctoral researcher in Professor Allen's group at The Ohio State University. Currently, Dr. Liu works as a design engineer in the field of civil/environmental engineering. Dr. Liu's research interests are focused on interfacial phenomena related to environmental processes and stormwater management/treatment technologies.

larization dependence of the SHG signal intensity locates the orientation of the molecular axis. Also very relevant to this review, recently Saykally and co-workers[7,8] used SHG to detect the presence of I^- ion, a strong nondirectional chromophore, at the aqueous interface. Mixtures lacking a dominant chromophore have many contributions from the various species to the second harmonic intensity, and they are, therefore, very challenging to analyze. A neat interface, such as water, has only one chromophore, and SHG has been used to determine the orientation of water molecules at the neat water interface.[11] The result is relevant to aqueous solution studies: the average water dipole moment vector is nearly parallel to the interface, and the hydrogen atoms are oriented slightly below the surface.

Compared with SHG, SFG is a somewhat more general technique that has become a popular choice for probing the

Heather C. Allen received her B.S. degree in Chemistry (1993) and her Ph.D. in Physical Chemistry (1997) at University of California, Irvine. Her undergraduate advisor was Professor F. S. Rowland (1995 Nobel Laureate), and her graduate advisor and coadvisor were Professors J. C. Hemminger and B. J. Finlayson-Pitts, respectively. She was funded through several fellowships: Fannie and John Hertz, EPA, and NSF Traineeship fellowships. Dr. Allen worked as a NOAA postdoctoral fellow in Climate and Global Change, which was awarded for her proposal based upon the use of nonlinear spectroscopy to study surfaces relevant to aerosol chemistry. Professor Allen was awarded the Research Innovation Award from Research Corp. in 2001, an OSU–OMA Distinguished Professional Mentor Award in 2001, an NSF CAREER Award in 2002, a Beckman Young Investigator Award in 2003, and an Alfred P. Sloan Award in 2005.

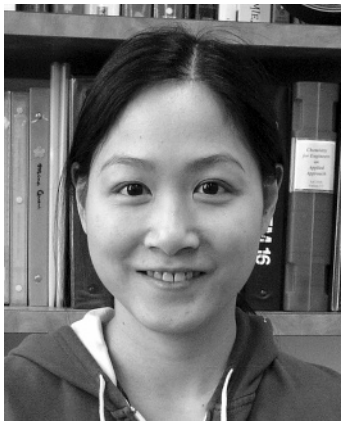

Margaret Kuo was born in Taipei, Taiwan, in 1978. She moved to Great Neck, New York, at the age of 13. She received her Bachelors degree in Chemistry from Tufts University and is continuing with her Ph.D. degree under the direction of Professor Mary Jane Shultz. She is currently working on water nanodrops in nonpolar solvents such as carbon tetrachloride. Her other interests include gourmet cooking, collecting arts and crafts from different countries, and employing her organizational talents wherever needed.

solution interface. As commonly implemented, SFG differs from SHG in consisting of two input beams—one visible and one infrared. In addition to varying the input polarizations, the infrared frequency is scanned (in some cases broad bandwidth infrared is used), and the intensity and polarization of the output beam are analyzed. The result is a polarization-dependent vibrational spectrum of the interface and, hence, contains species-specific orientation information. To demonstrate the applicability of the technique, the first SFG experiments, reported in 1987−88, optimized the surface concentration and limited subsurface penetration by examining organic molecules on solid substrates such as quartz[12,13] and semiconductors.[14] Later, Shen and co-workers[15] used SFG to study the neat methanol liquid interface, and in 1993, they reported the first SFG spectrum of the pure water

Mary Jane Shultz was born in Cosmos, Minnesota, a small rural town. She is a 1970 Honors graduate of the University of Wisconsin, Madison, and received her Ph.D. in theoretical chemistry from Massachusetts Institute of Technology under the direction of Prof. Robert Silbey. She was a postdoctoral fellow of the Radcliffe Institute and the Division of Engineering and Applied Physics at Harvard University under the direction of Professor Nicholas Bleombergen. She is presently Professor and Chair of the Chemistry Department at Tufts University. Her current research focuses on application of nonlinear spectroscopy to issues relating to water at interfaces: aqueous solutions, metal oxide surfaces, and solid water interfaces. She is an avid skier, tennis player, gourmet cook, and gardener.

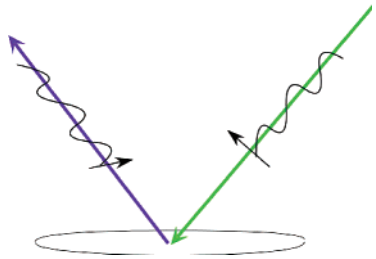

Figure 1. Schematic of second harmonic generation. In the illustration, a *p* polarized visible beam interacts with surface molecules to generate an *s* polarized output beam.

interface.[16] Currently, SFG is the only technique capable of selectively producing vibrational spectra of neat liquid interfaces, liquid/air solution interfaces, or buried liquid/liquid interfaces.[1,17−22]

The basis for SFG is as follows. When a light beam impinges on a surface, it induces a polarization by exerting a force on the valence electrons. In first order, the medium responds linearly to the incident field, producing absorption or Rayleigh or Raman scattering. If the incident field is sufficiently intense, the medium responds nonlinearly and this response is described by the hyperpolarizability of the medium.[23−28] To second order, the incident electric fields produce electric fields $\mathbf{E}_1$ and $\mathbf{E}_2$ in the medium that induce a polarization, $\mathbf{P}$

$$\mathbf{P} = \alpha^{(1)}\cdot\mathbf{E}_1 + \chi^{(2)}:\mathbf{E}_1\mathbf{E}_2 \qquad (1)$$

where $\alpha^{(1)}$ and $\chi^{(2)}$ are the linear polarizability and the hyperpolarizability, respectively. The $\chi^{(2)}$ term gives rise to SHG, SFG, and difference frequency generation (DFG). $\chi^{(2)}$ is a tensor which is the focus of this discussion. The observed intensity, $\mathbf{I}$, is related to the absolute square of the polarization, $\mathbf{P}$, modulated by a nonlinear Fresnel coefficient.[9] The square is the source of interferences that can be used to determine the absolute orientation (up versus down) via reference to a known surface[29−32] or to determine the orientation of one chromophore relative to another.[33]

Equation 1 implies that two relationships determine the second-order response. One is the relationship of the electric fields, $\mathbf{E}_1$ and $\mathbf{E}_2$, in the medium to the incident fields and the analogous relationship between the induced polarization, $\mathbf{P}$, and the electric field of the observed signal. These relationships are given by linear and nonlinear Fresnel coefficients, respectively. The second relationship is that between the macroscopic hyperpolarizability tensor, $\chi^{(2)}$, and the molecular hyperpolarizability since this sheds light on the orientation of the interfacial molecules. Each of these relationships is described below.

2.1. Optical Factors and Electric Fields

The electric fields in the medium are related to the incident fields by Fresnel factors that reveal the efficiency for coupling the incident field into the interface. There is a similar optical factor for coupling out the generated polarization to produce the sum frequency. These factors result from the boundary condition that the tangential component of the electric field is continuous across a boundary.[9] The two electric fields, $\mathbf{E}_J$ and $\mathbf{E}_K$, in the medium are related to the input fields, $e_1{}^\circ_{vis}$ and $e_2{}^\circ_{vis}$, by

$$E_J(\mathrm{vis}_1) = K_J(\mathrm{vis}_1)e_1{}^\circ_{vis};\quad E_K(\mathrm{vis}_2) = K_K(\mathrm{vis}_2)e_2{}^\circ_{vis} \qquad (2)$$

for SHG if two different polarization input beams are used. With a single input polarization, $\mathbf{E}_J$ and $\mathbf{E}_K$ are equal. For SFG, the electric fields in the medium are given by

$$E_J(\mathrm{vis}) = K_J(\mathrm{vis})e^\circ_{vis};\quad E_K(\mathrm{IR}) = K_K(\mathrm{IR})e^\circ_{IR} \qquad (3)$$

The Fresnel factors K_J(vis) and K_K(IR) are listed in Table 1, and e°_{vis} (e°_{IR}) is the incident visible (infrared) field. A similar nonlinear optical factor, L_l(SF) (Table 1), describes coupling of the generated sum frequency (or second harmonic, L_l(SH)) out of the medium. The Fresnel factors have the effect of reducing the incident electric fields.

The observed intensity depends on the polarizations of the sum frequency and the two incident beams. (For simplicity, the following discussion is limited to SFG. SHG analysis is analogous.) By convention, the surface normal is *Z* and the surface plane is the *XY* plane. The beam polarization is given with respect to the *XYZ* coordinate system. The plane of incidence is defined as the plane containing the surface normal and the propagation direction of the beam. Most often, the visible and infrared beams are coplanar, so this will be assumed. (Noncoplanar input planes are possible[25]

Table 1. Fresnel Factors[1,24] [a]

	L_l(SF)	K(vis)	K(IR)
X	$-\cos\theta_{t,SF}/[\cos\theta_{t,SF} + n_{SF}\cos\theta_{i,SF}]$	$2\cos\theta_{i,\omega1}\cos\theta_{t,\omega1}/[\cos\theta_{t,\omega1} + n_1\cos\theta_{i,\omega1}]$	$2\cos\theta_{i,\omega2}\cos\theta_{t,\omega2}/[\cos\theta_{t,\omega2} + n_2\cos\theta_{i,\omega2}]$
Y	$1/[\cos\theta_{i,SF} + n_{SF}\cos\theta_{t,SF}]$	$2\cos\theta_{i,\omega1}/[\cos\theta_{i,\omega1} + n_1\cos\theta_{t,\omega1}]$	$2\cos\theta_{i,\omega2}/[\cos\theta_{i,\omega2} + n_2\cos\theta_{t,\omega2}]$
Z	$-\sin\theta_{t,SF}/[\cos\theta_{t,SF} + n_{SF}\cos\theta_{i,SF}]$	$-2\cos\theta_{i,\omega1}\sin\theta_{t,\omega1}/[\cos\theta_{t,\omega1} + n_1\cos\theta_{i,\omega1}]$	$-2\cos\theta_{i,\omega2}\sin\theta_{t,\omega2}/[\cos\theta_{t,\omega2} + n_2\cos\theta_{i,\omega2}]$

[a] *X*, *Y*, and *Z* are the laboratory coordinates, where *XZ* is the plane of incidence and *XY* is the surface plane. θ_i = incident angle, θ_t = transmitted angle, and n_m is the refractive index of the medium at frequency ω_m. (The refractive index of air is assumed to be unity at all wavelengths.)

and sometimes dictated by other experimental criteria; the direction of the sum frequency beam is determined by momentum matching and is in neither the infrared nor the visible planes of incidence.) Polarization is defined by the input plane: polarization in the plane of incidence is *p* polarized; that perpendicular to the plane of incidence is *s* polarized. The three polarizations are specified as subscripts in the order: sum frequency, visible, and infrared. For example, the *ssp* intensity is that generated with *s* polarization from an *s* polarized visible beam and a *p* polarized infrared beam. The intensities are related to the incident fields and the Fresnel coefficients as follows:

$$I_{ssp} \propto |L_Y \chi_{YYZ} K_Y^{\mathrm{vis}} K_Z^{\mathrm{IR}} e_{\mathrm{vis}}^{s} e_{\mathrm{IR}}^{p}|^2$$

$$I_{sps} \propto |L_Y \chi_{YZY} K_Z^{\mathrm{vis}} K_Y^{\mathrm{IR}} e_{\mathrm{vis}}^{p} e_{\mathrm{IR}}^{s}|^2$$

$$I_{pss} \propto |L_Z \chi_{ZYY} K_Y^{\mathrm{vis}} K_Y^{\mathrm{IR}} e_{\mathrm{vis}}^{s} e_{\mathrm{IR}}^{s}|^2$$

$$I_{ppp} \propto |L_X \chi_{XXZ} K_X^{\mathrm{vis}} K_Z^{\mathrm{IR}} e_{\mathrm{vis}}^{p} e_{\mathrm{IR}}^{p} + L_X \chi_{XZX} K_Z^{\mathrm{vis}} K_X^{\mathrm{IR}} e_{\mathrm{vis}}^{p} e_{\mathrm{IR}}^{p} + L_Z \chi_{ZXX} K_X^{\mathrm{vis}} K_X^{\mathrm{IR}} e_{\mathrm{vis}}^{p} e_{\mathrm{IR}}^{p} + L_Z \chi_{ZZZ} K_Z^{\mathrm{vis}} K_Z^{\mathrm{IR}} e_{\mathrm{vis}}^{p} e_{\mathrm{IR}}^{p}|^2 \quad (4)$$

For sum frequency, the first two subscripts reference the Raman process, so $\chi_{YZY} = \chi_{ZYY}$ and I_{sps} differs from I_{pss} only in a multiplicative factor due to the combination of Fresnel factors. The aqueous solution interface is isotropic in the surface plane, so $\chi_{YYZ} = \chi_{XXZ}$, $\chi_{YZY} = \chi_{XZX}$, $\chi_{ZYY} = \chi_{ZXX}$, and χ_{ZZZ} is unique. Thus, there are four unique polarizibility elements. Orientation at the aqueous interface usually results in the highest intensity for the *ssp* polarization combination.

As a coherent process, the sum frequency beam is generated at a well-defined angle, θ_{SF}, determined by momentum matching at the interface:

$$n_{\mathrm{SF}} \omega_{\mathrm{SF}} \sin\theta = n_1 \omega_1 \sin\theta_1 \pm n_2 \omega_2 \sin\theta_2 \quad (5)$$

The plus sign is used when the incident beams are from the same side of the interface. The negative sign is used when the incident beams are from opposite sides of the interface.[9] Momentum matching dictates that the sum frequency signal is generated between the infrared and visible reflected beams, which facilitates spatial filtering of the three beams (sum frequency, visible, and infrared).

2.2. Nonlinear Susceptibility and Orientation

The nonlinear susceptibility, χ_{IJK}, describes the surface polarization response to the electric fields of the incident light beams. It consists of a contribution from the induced electronic polarization and the vibrational dipole of the bonded groups on the surface averaged over molecules within the coherence length—a length on the order of the shortest incident wavelength. χ_{IJK} is determined by averaging the molecular hyperpolarizability, $\beta_{\alpha\beta\gamma}$, over the molecular orientations.

$$\chi_{IJK} = N\langle\beta_{\alpha\beta\gamma}\rangle \quad (6)$$

where N is the number of oscillators contributing to the signal and $\langle ... \rangle$ denotes the orientational average. $\chi^{(2)}$ is the average projection of the molecular hyperpolarizability onto the incident light fields. Practical calculation of $\chi^{(2)}$ involves determining the Euler angle relationships among four coordinate systems: the laboratory system (*XYZ*) that defines the plane of incidence, the surface system (*xyz*) that defines the surface normal, the molecular Cartesian system (*abc*), and the molecular normal coordinates (*ABC*). In eq 6, *I*, *J*, and *K* represent *X*, *Y*, or *Z*, and α, β, and γ represent *a*, *b*, or *c*. The general relationships among the χ_{IJK} and the $\beta_{\alpha\beta\gamma}$ parameters are lengthy and given in the literature.[24,34,35] Often, the symmetry of the molecule or the normal mode considerably simplifies these relationships.

There are 27 elements of the molecular hyperpolarizibility tensor. Often this number is reduced by the symmetry of the molecule under consideration (in addition to the symmetry of the surface). For example, a water molecule has C_{2v} symmetry and has only five nonzero elements in the hyperpolarizability tensor: β_{caa}, β_{aca}, β_{aac}, β_{bbc}, and β_{ccc}. Of these only β_{bbc}, β_{aac}, and β_{ccc} are nonzero for the symmetric stretch and β_{caa} and β_{aca} are nonzero for the antisymmetric stretch. Let θ be the tilt angle between the molecular C_2 axis and the surface normal and let ϕ be the twist angle of the molecular plane with respect to the surface plane. Then, the relationship between the molecular hyperpolarizibility, $\beta^{(2)}$, and the macroscopic hyperpolarizibility, $\chi^{(2)}$, for the symmetric stretch (after Euler angle transformations from the molecular coordinates, $\alpha\beta\gamma$, to the surface, *ijk*, and then to the laboratory coordinates, *IJK*) *is*

$$\chi_{xxz} = {}^1/_2\{\cos\theta(\beta_{aac} + \beta_{bbc}) - (\cos\theta - \cos^3\theta)(\cos^2\phi\beta_{aac} + \sin^2\phi\beta_{bbc} - \beta_{ccc})\}$$

$$\chi_{xzx} = {}^1/_2(\cos\theta - \cos^3\theta)\{\beta_{ccc} - \cos^2\phi\beta_{aac} - \sin^2\phi\beta_{bbc}\}$$

$$\chi_{zxx} = {}^1/_2(\cos\theta - \cos^3\theta)\{\beta_{ccc} - \cos^2\phi\beta_{aac} - \sin^2\phi\beta_{bbc}\}$$

$$\chi_{zzz} = \cos^3\theta\beta_{ccc} + (\cos\theta - \cos^3\theta)[\cos^2\phi\beta_{aac} + \sin^2\phi\beta_{bbc}] \quad (7)$$

For the antisymmetric stretch, it is

$$\chi_{xxz} = -(\cos\theta - \cos^3\theta)\cos^2\phi\beta_{caa}$$

$$\chi_{xzx} = {}^1/_2\{(1 - 2\sin^2\theta\cos^2\phi)\cos\theta\}\beta_{caa}$$

$$\chi_{zxx} = {}^1/_2\{(1 - 2\sin^2\theta\cos^2\phi)\cos\theta\}\beta_{caa}$$

$$\chi_{zzz} = 2(\cos\theta - \cos^3\theta)\cos^2\phi\beta_{caa} \quad (8)$$

The result for the symmetric stretch of a molecule with C_{3v} symmetry is the same as that for one with C_{2v} symmetry with the simplification that $\beta_{aac} = \beta_{bbc}$. The antisymmetric stretch is slightly more involved due to the degeneracy of the normal mode. Projecting the normal mode susceptibility onto the Cartesian susceptibility involves determining the average projection of the normal coordinates onto the molecular Cartesian coordinate system:

$$\beta_{\alpha\beta\gamma} = \frac{1}{n_{\mathrm{orientations}}} \sum \beta_{ABC} \quad (9)$$

where n is the number of equivalent orientations. The result is

$$\chi_{xxz} = -^1/_2 \sin^3\theta \cos 3\phi\beta_{aaa} - (\cos\theta - \cos^3\theta)\beta_{caa}$$

$$\chi_{xzx} = -^1/_2 \sin^3\theta \cos 3\phi\beta_{aaa} + \cos^3\theta\beta_{caa}$$

$$\chi_{zxx} = -^1/_2 \sin^3\theta \cos 3\phi\beta_{aaa} + \cos^3\theta\beta_{caa}$$

$$\chi_{zzz} = \sin^3\theta \cos 3\phi\beta_{aaa} + 2(\cos\theta - \cos^3\theta)\beta_{caa} \quad (10)$$

2.3. Observed Intensity—Interference

For a two-dimensional, isotropic surface such as the aqueous interface, the orientational average results in zero intensity for *sss*, *spp*, *psp*, and *pps* polarizations. Most of the studies discussed below use the *ssp* polarization combination, so the SFG intensity is strongly affected by the projection of the infrared dipole onto the surface normal.

The SFG signal intensity is proportional to the polarization squared

$$\text{signal intensity, } I^{v}_{\text{SFG}} \propto |P|^2 \propto |\chi^{(2)}_v|^2 = N^2|\langle\beta^{(2)}\rangle|^2 \quad (11)$$

and thus, the SFG intensity is proportional to the square of the number of molecules contributing to the signal modulated by the average orientation. The molecular susceptibility can be described by eq 12,

$$\beta_{\alpha\beta\gamma,v} = \frac{\langle g|\alpha_{\alpha\beta}|v\rangle\langle v|\mu_\gamma|g\rangle}{\omega_{\text{IR}} - \omega_v + i\Gamma_v} \quad (12)$$

where $\langle g|\alpha_{\alpha\beta}|v\rangle$ defines the Raman tensor for the transition and $\langle v|\mu_\gamma|g\rangle$ defines the IR transition moment for the molecule. For a single vibrational mode, we can ignore phase; thus, from eqs 11 and 12, we have

$$I^{v}_{\text{SFG}} \propto N^2|\sum_{\alpha\beta\gamma}\langle\mu_{IJK:\alpha\beta\gamma}\rangle\langle g|\alpha_{\alpha\beta}|v\rangle\langle v|\mu_\gamma|g\rangle|^2 \quad (13)$$

where $\mu_{IJK:\alpha\beta\gamma}$ is the Euler angle transformation between the laboratory coordinates (I, J, K) and the molecule coordinates (α, β, γ). Equation 13 relates the SFG intensity to the Raman tensor times the IR transition moment (the separate square of each integral is the corresponding intensity) for a single vibrational mode.

2.3.1. Spectral Fits

In addition to the resonant susceptibility, $\chi^{(2)}_v$, $\chi^{(2)}$ contains a nonresonant term as shown in eq 14

$$|\chi^{(2)}|^2 = |\chi^{(2)}_{\text{NR}} + \sum_v \chi^{(2)}_v|^2 \quad (14)$$

The nonresonant signal from a material with known $\chi^{(2)}_{\text{NR}}$ can be used to determine the unknown phase for the medium under investigation and, therefore, the orientation of molecules at an interface. The first demonstration of the use of a reference to determine orientation is that of Eisenthal, Heinz, and co-workers.[32] Using the nonresonant signal from a quartz reference and SHG, these researchers determined the absolute orientation of water molecules at the aqueous interface. The analysis of the spectra revealed that the hydrogen atoms point slightly into the bulk. More recently, Shen *et al.*[31] have used the nonresonant signal from quartz and SFG to determine the orientation of water molecules at the quartz interface as a function of pH for the multiple components of the hydrogen-bonded absorption of water. (This result is discussed further below.)

The SFG spectrum, which is a plot of the SFG intensity (I_{SFG}) as a function of the incident infrared frequency (ω_v), can be mathematically fit according to eq 14, where $\chi^{(2)}_v$ is given below

$$\chi^{(2)}_v \propto \frac{A_v}{\omega_v - \omega_{\text{IR}} - i\Gamma_v} \quad (15)$$

$$\chi^{(2)}_v \propto \left\langle \sum_v \frac{\langle g|\alpha_{ab}|v\rangle\langle v|\mu_c|g\rangle}{\omega_v - \omega_{\text{IR}} - i\Gamma_v} \right\rangle = \left\langle \sum_v \frac{A_v}{\omega_v - \omega_{\text{IR}} - i\Gamma_v} \right\rangle \quad (16)$$

A_v is the amplitude of the SFG transition moment, ω_v is the frequency, and Γ_v is the line width of the transition.

For aqueous solutions, a constant, complex nonresonant $\chi^{(2)}_{\text{NR}}$ is used and the sign of the amplitude (A_v) denotes the phase of the vibrational mode from the interfacial molecules, which incorporates orientation and relative vibrational phases. The combination of eqs 14 and 15 indicates a Lorentzian line shape. In Raman and IR spectroscopy, the overall intensity is the summation of the intensity of each vibration, while in SFG the intensity is proportional to the absolute square of the summation of the $\chi^{(2)}_v$ and $\chi^{(2)}_{\text{NR}}$ of each vibration as shown in eq 14. The square of the sum leads to interferences in SFG spectra that are not present in Raman or IR spectra. Therefore, SFG intensity analysis must occur after deconvolution into the component peaks since direct comparison of SFG spectra to Raman and IR spectra may be misleading, in particular for broad, overlapping bands.

2.4. Experimental Section

The experimental objective is to overlap pulsed visible and infrared beams in space and time on the liquid interface. The source of the pulsed visible beam commonly varies with pulse duration. A Nd:YAG laser is often used for nanosecond or picosecond (>10 ps) studies while picosecond (<10 ps) or femtosecond studies use a Ti:sapphire laser. The infrared beam can be generated by Raman shifting in high-pressure hydrogen[36−39] or using a solid-state optical parametric oscillator/optical parametric amplifier (OPO/OPA) (nanosecond), an optical parametric generator/optical parametric amplifier (OPG/OPA) (picosecond), or, typically with white light generation for a broad band OPG/OPA (femtosecond). The polarization of both the visible and infrared beams is rotated as required. Typically**, t**he two beams are focused at or near the liquid interface in a coplanar geometry. Focusing parameters can vary depending on the experimental setup. Spectra are normalized to the infrared intensity and often referenced to a signal from a standard.

3. Results and Discussion

3.1. Spectroscopy—Spectral Assignments of Neat Water

This review discusses water structure as influenced by various electrolytes or ammonia; therefore, we first discuss the SFG spectrum of the air/water interface itself. The SFG spectrum with *ssp* polarization, in the OH stretch region of

the air/neat water interface, and the isotropic Raman and ATR-FTIR spectra of neat water are shown in the figures that follow. There are a number of groups that have published neat water SFG spectra,[16,22,40−46] and all of these published spectra are relatively similar to one another. Differences in the SFG spectra arise mainly from the individual SFG system and varying pulse energies, repetition rates, pulse stability, infrared profiles, and optimization conditions from lab to lab. These instrumental differences have little impact on the interpretation of surface water spectra. Interpretation differences arise from the broadness of the hydrogen-bonding region; the component peaks may be varied substantially while still retaining the overall fit. The narrow peak at 3700 cm^{-1}, first revealed by Shen and co-workers,[16] is unambiguously the dangling OH from surface water molecules, and there is no debate on this SFG spectral designation.

We next address spectral assignments for the hydrogen-bonded region, shown in Figure 2, for bulk and surface water, pointing out similarities and differences. The broad peaks in the 3000−3600 cm^{-1} region contain two prominent bands in the SFG, the Raman, and the IR spectra of neat water and are positioned at ∼3200 and ∼3450 cm^{-1}. Generally following spectral assignments for ice[47] and considering the increase in disorder of a noncrystalline system, the 3200 cm^{-1} peak in the Raman (3253 cm^{-1}) and IR (3215 cm^{-1}) spectra is attributed to vibrational modes from the four oscillating dipoles associated with four-coordinate, hydrogen-bonded water molecules. These collective vibrations can be viewed as possessing symmetric character. In the bulk, there is a dominant contribution from these four-coordinate molecules. However, due to truncation of tetrahedral bonding at the surface, there is a minimal contribution from four-coordinate interfacial oscillating dipole modes in the SFG peak at ∼3200 cm^{-1} of neat water. Rather, this peak is attributed predominantly to the three-coordinate water molecules at the surface that are single proton donor/double proton acceptor (DAA) molecules.[48−51] DAA water molecules have the strongest perturbation of the donor OH oscillator due to the hydrogen bonding; that is, they have the strongest hydrogen bond and are thus shifted furthest from the unperturbed, gas-phase OH stretch. Previous interpretations of the 3200 cm^{-1} band in SFG spectra of neat water have discussed this hydrogen-bonded region as possessing "icelike" character; however, this interpretation is not consistent with the evolving picture of the neat water surface, which does not include analogous ice structural ordering. In recent work,[43] the 3200 cm^{-1} band is now attributed to the vibrations of OH oscillators that are from surface water molecules that have one completely free OH (the 3700 cm^{-1} OH oscillator) and one OH that is hydrogen bonded to other water molecules (i.e. the other end of the free OH), the DAA water molecules. This new interpretation is based on cluster studies[48,50,52] that have provided compelling evidence that, prior to adding a solute or electrolyte to water, the air/water interface is relatively shallow. This narrow transition zone from the vapor state to the bulk liquid state is also supported by several theoretical studies.[6,53]

In the Raman, IR, and SFG spectra, the 3450 cm^{-1} peak is attributed to the more asymmetrically oscillating dipoles from four-coordinate hydrogen-bonded water molecules. This spectral region can also be described as arising from four-coordinate water molecules where one hydrogen is a poor hydrogen bond donor. It is important to note here that these assignments continue to be discussed and are not entirely

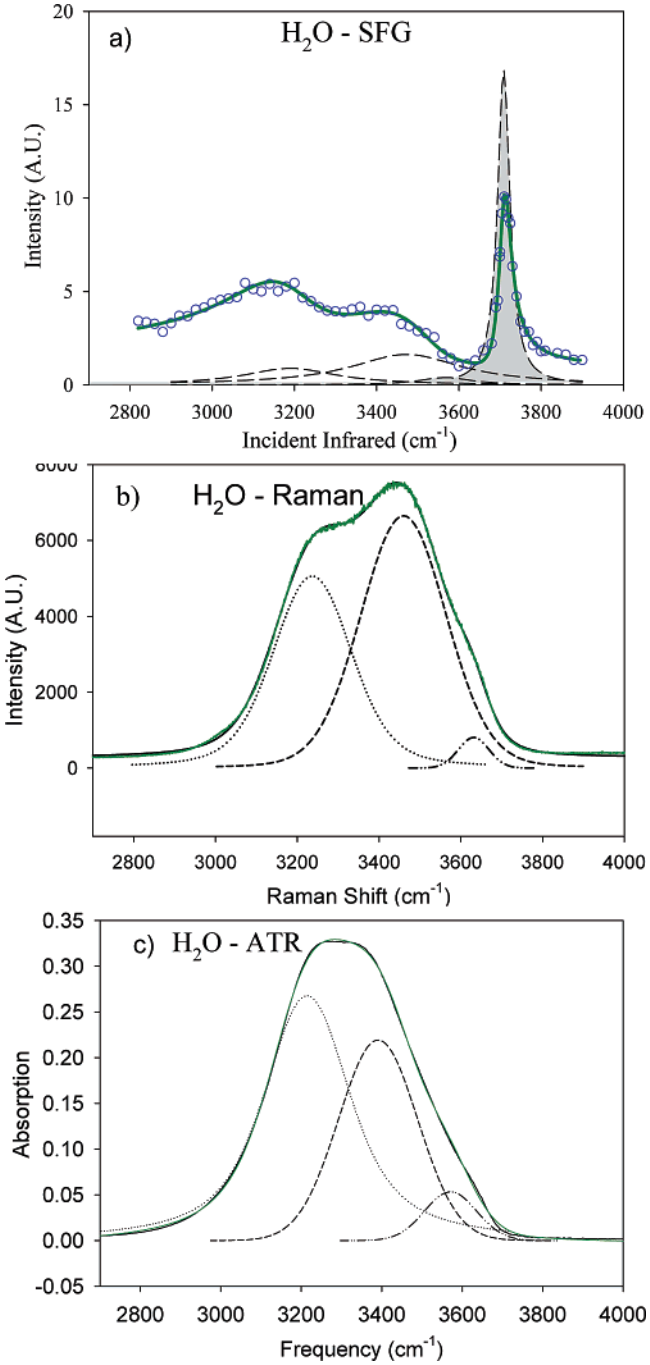

Figure 2. (a) SFG *ssp* polarized spectrum of neat water in the O−H stretching region (the deconvoluted peaks shaded in gray have "−" phase while those which are not shaded have "+" phase). (b) Isotropic Raman spectrum of neat water. (c) ATR−IR spectrum of neat water. The calculated spectra from the spectral fits are shown in green. All spectra were taken at ∼24 °C. Reprinted with permission from ref 43. Copyright 2005 American Chemical Society.

agreed upon within the scientific community. The smaller peak at ∼3550 cm^{-1} in the SFG, Raman (3630 cm^{-1}), and IR (3571 cm^{-1}) spectra[54,55] is assigned to the modes associated with three-coordinate asymmetrically hydrogen-bonded water molecules in which one OH bond is involved in strong hydrogen bonding and the other is only weakly hydrogen bonded.[54] For the SFG, these three-coordinate species are double proton donor/single proton acceptor (DDA) molecules.[48−51] The possibility of a Fermi resonance between the second overtone of the water bend and the OH

stretches has been debated intensely in the literature (see, for example, Chapter 3 in ref 54). While this resonance probably does contribute to the observed intensity in the SFG spectrum of water, it is expected to be small.

The narrow peak at 3700 cm^{-1} in the SFG spectrum,[16,41,42] as briefly discussed above, is assigned to the dangling (i.e. surface) OH stretch of water molecules that span the interface in which one non-hydrogen-bonded OH is directed into the vapor phase.[16,41,42] The other OH, interacting through hydrogen bonding with the liquid phase as described above, is within the ~3200 cm^{-1} peak.[43,49−51]

The assignment of the component peak at ~3750 cm^{-1} in the SFG spectrum of neat water is still under debate; however, recent discussions point to potential origins. One is a combination of the 400 cm^{-1} and the 3400 cm^{-1} modes as suggested by infrared bulk water analysis.[56] Another reasonable explanation for the blue-shifted intensity adjacent to the free OH is surface water distortion, possibly the less than optimal tetrahedral hydrogen-bonding substructure as discussed in cluster studies.[49] This latter assignment is supported by the aqueous ammonia studies, discussed later in this review. Additionally, recent works by Johnson, Jordan, and co-workers,[57] Duncan and co-workers,[58] and McCoy[58] support the existence of a higher frequency peak in water clusters. The Johnson and Jordan and co-workers research shows that there are two peaks at ~3700 cm^{-1} and ~3720 cm^{-1} in the infrared spectra of water clusters. The low-frequency peak is assigned to the free OH stretch of DAA water molecules as stated above, while the high-frequency peak is assigned to two-coordinate DA water molecules. Two- and three-coordinate water molecules were also identified as surface species in amorphous ice in previous work by Buch and Devlin.[59] It is important to note that improper normalization techniques can account for a significant portion of the 3750 cm^{-1} intensity in many studies; however, even after correct normalization, intensity remains in this region.

In summary, the detailed spectral assignments for the SFG spectrum of the air/neat water interface are nontrivial because of the dynamic nature of the hydrogen bond. However, the above-mentioned experimental and theoretical works shed light on the main contributions. For the SFG, Raman, and IR spectral assignments of neat water, as the frequency increases, the hydrogen-bonding strength decreases. In addition, as the frequency increases, the asymmetric character of the modes increases.

3.2. Salts

Dissolved salts are known to affect the structure of water through solvation of the ions by water molecules. Water molecules surround the anions and cations to solvate them, effectively shielding their charges. Specifically, the effect of charge, polarizability, and size of the ions, particularly the anions, has been extensively studied in the literature.[6,43,44,60−63] In this section, the effect of salts on the surface structure of water is explored. Perturbations to the air/water interface are not easily predicted from bulk aqueous solution studies. Water molecules within the air/water interface solvate these ions differently than in the bulk. The interface becomes its own phase with varying characteristics relative to both the gas and the liquid phases.We discuss the evidence supporting a model of the interface changing its depth; that is, the interfacial zone widens, creating a nonbulk zone that is wider than one might expect due to changing concentrations and changing concentration profiles.

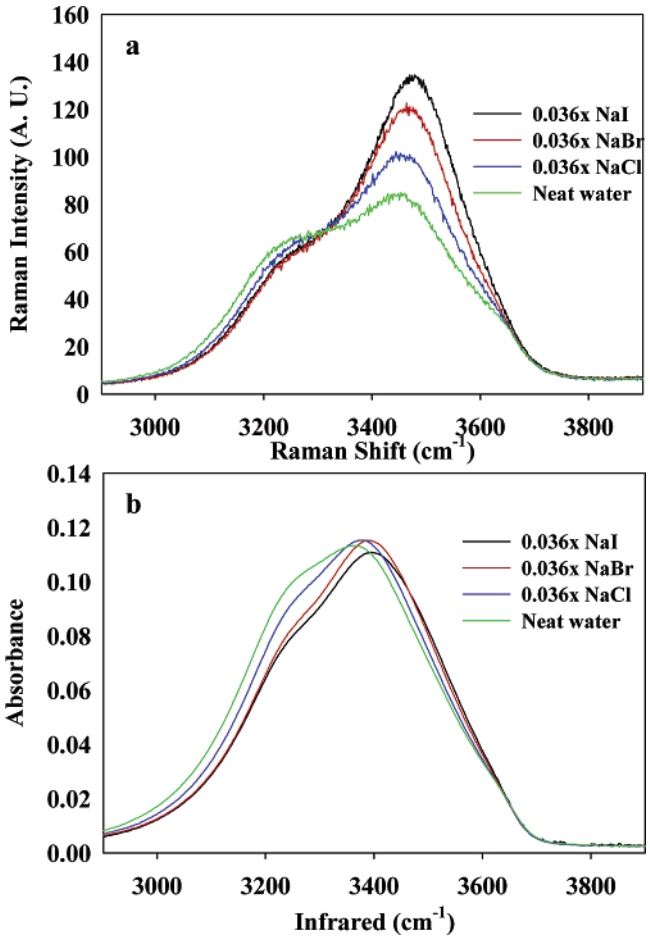

Figure 3. (a) Raman and (b) ATR-FTIR spectra of neat water and sodium halide solutions. $T \sim 24$ °C. Reprinted with permission from ref 44. Copyright 2004 American Chemical Society.

In the next subsections, we explore the recent literature relevant to the structure of interfacial water with several types of salts ranging from sodium halides, to ammonium and sulfate salts, to bisulfate salts.

3.2.1 Sodium Halides

The studies of halide salts at aqueous interfaces have generated great interest because of recent understanding of the heterogeneous ozone chemistry in the marine boundary layer.[64−68] These studies postulate that chloride anions must be present at the air/water interface in order to account for the measured oxidation reaction rates. However, according to conventional wisdom, ions are repelled from surfaces, as reflected by surface tension measurements of numerous aqueous inorganic salt solutions, which show that the salts raise the surface tension of water. This implies, via the Gibbs adsorption equation,[69] that there is a net surface deficit of ions.

Raman and infrared spectra provide information on the bulk structure of water.[61,62,70,71] Since the interface is the transition zone between the bulk condensed phase and its vapor phase, it is necessary to discuss the bulk spectra. Additionally, SFG spectra are interpreted by utilizing the relationship between SFG and Raman and IR intensities as discussed in section 2.3. As shown in Figure 3,[6,44] relative to the neat water spectra, the Raman and IR spectra reveal a decrease in the 3200 cm^{-1} band, and most of the intensity loss can be correlated to the displacement of the water molecules in the symmetric hydrogen-bonding network by

the sodium cation and the halogen anion (iodide being the largest). However, in the Raman spectrum enhancement of the 3450 cm^{-1} peak dominates, and this is not observed in the IR spectra. With the addition of salts containing anions of increasing polarizability ($I^- > Br^- > Cl^- > F^-$), electrons of the OH bonds in the water molecules that solvate these anions shift, resulting in an increased polarizability. Thereby, the solvation sphere water molecules, which are observed in the asymmetric hydrogen-bonding network, exhibit this polarizability change in the Raman spectra since Raman intensities arise from this phenomenon.[72] The change in the polarizability of the OH bonds of water molecules from the halide anion solvation environment was also suggested by IR vibrational femtosecond pump/probe experiments.[73,74]

Sum frequency generation spectroscopy probes the vibrational transition moments that are both IR and Raman active. As shown in Figure 4, SFG spectra of 0.036*x* sodium chloride aqueous solutions overlap with that of neat water,[44,75,76] while an enhanced feature is observed around 3450 cm^{-1} for NaBr and NaI. The intensity of this peak increases from NaF to NaI.[44,76] Although the spectral fitting routine and data analysis techniques used in each of these studies are quite different, the common conclusion drawn is that halide anions perturb the interfacial water structure and, hence, must be present at the air/aqueous interface.

We now address the question of what is the interface. The interface is defined by the concentration gradients of the different species and lacks an inversion center (and is, hence, SFG active), while the bulk is defined as the region where the species are homogeneously mixed and, therefore, has a macroscopic center of inversion (and is, hence, SFG inactive).

SFG studies on aqueous halide interfaces by Liu *et al.*[44] were compared to bulk vibrational spectra of these solutions (Raman and IR). The bulk water structures for the sodium fluoride and chloride aqueous solutions are found to be similar to the air/water interface in the four-coordinate hydrogen-bonded stretching region, whereas sodium bromide and iodide cause significant distortion of the hydrogen-bonding network in the bulk, manifested in the increase in intensity in the 3450 cm^{-1} peak in the Raman and IR spectra. A comparison between the interfacial and bulk structures of water can be made as shown in Figure 5. This figure shows a comparison of the integrated peak intensities in the hydrogen-bonded region of water from the fits of the SFG spectra with the corresponding product of the fitted Raman intensity times the IR intensity (recall that, for an isolated vibrational mode and neglible nonresonant background, the SFG intensity is proportional to the Raman intensity times the IR intensity as per section 2.3). The enhanced SFG intensity is interpreted as being due to an increase in the interfacial depth in the NaBr and NaI aqueous solutions as compared to neat water, NaF, and NaCl. The increase in interfacial depth implies that there are concentration gradients of the various species that extend the interfacial region several layers into what was the bulk (and, thus, increase the number of water molecules that are SFG active).

These results are consistent with the recent MD simulations[53,77] that reveal an increase in interfacial depth upon addition of sodium halides to water, that is, density gradients that extend over a larger region. Additionally, by using a series of $HOD/H_2O/D_2O$[78] halide aqueous solutions, Raymond *et al.*[76] suggested that ions in the topmost layer do not cause a measurable change in the hydrogen bonding

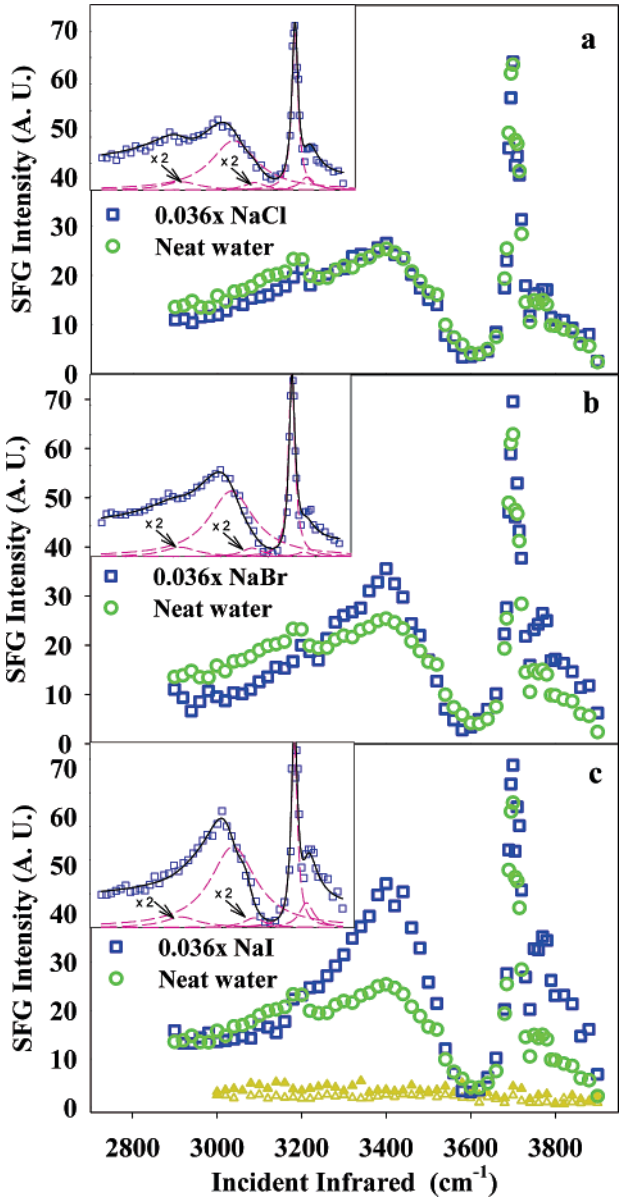

Figure 4. *ssp* polarized SFG spectra (taken at ~24 °C) of (a) 0.036*x* NaCl, (b) 0.036*x* NaBr, and (c) 0.036*x* NaI. The neat water SFG spectrum is plotted in each figure for comparison. The open yellow and closed yellow triangles within part c show the sum frequency intensity of the 0.015*x* NaI in D_2O and pure D_2O, respectively. Insets: SFG sodium halide aqueous solution spectral fits. Component Lorentzian peaks are shown as dashed pink lines, and the calculated fits from the component peaks are shown as black lines that go through most of the data points. Reprinted with permission from ref 44. Copyright 2004 American Chemical Society.

between these interfacial water molecules, and the total interfacial ion concentration is lower than that of the bulk. Overall, the SFG spectra reported[44,75,76] are qualitatively in agreement with each other and support the MD simulation results, revealing the presence of Br^- and I^- in the interfacial region as shown in Figure 6.

Other surface-sensitive techniques, such as extended X-ray adsorption fine structure (EXAFS) spectroscopy and X-ray photoelectron spectroscopy (XPS), provide direct experimental approaches to further describe the interface. In a recent study by Ghosal *et al.*,[79] the composition of the liquid/vapor interface for deliquesced samples of potassium bromide and potassium iodide was measured using X-ray photoelec-

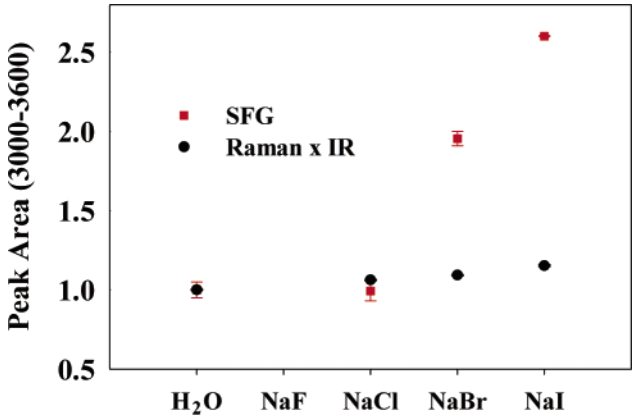

Figure 5. Areas of the 3250, 3450, and 3550 cm^{-1} (approximate, positions varied) peaks in the OH stretch region for Raman × infrared (Raman area multiplied by ATR-FTIR area) and SFG. Areas were normalized to neat water for 0.036*x* solutions. The interfacial depth has increased for the NaBr and NaI aqueous solutions; that is, more water molecules are contributing to the SFG intensity of the NaBr and NaI solutions as compared to the cases for neat water and NaF and NaCl solutions. Reprinted with permission from ref 44. Copyright 2004 American Chemical Society.

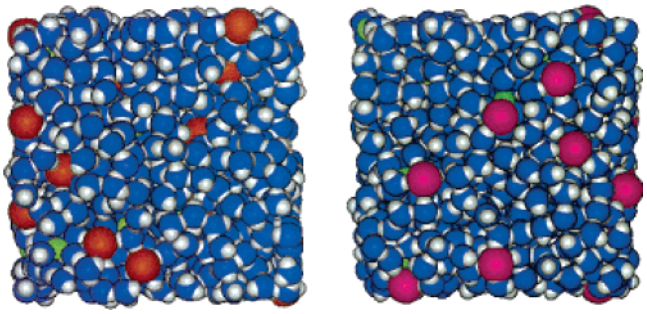

Figure 6. Snapshots of molecular dynamic simulations for (a) 0.02*x* (1.2 M) NaBr and (b) 0.02*x* (1.2 M) NaI solution surfaces: orange, Br^-; red, I^-; green, Na^+; blue, O; gray, H. Reprinted with permission from ref 125. Copyright 2000 American Chemical Society.

tron spectroscopy operating at near ambient pressure. The XPS spectra indicate that the surface composition of the saturated solution is enhanced in the halide anion compared to the bulk. Moreover, the enhancement of the anion concentration is more dramatic for the larger, more polarizable iodide anion. The XPS results are in good qualitative agreement with classical molecular dynamics simulations. Additionally, the work by Peterson and Saykally[80] also supports the existence of I^- in the interfacial region of water through a direct SHG measurement of the I^- anion.

3.2.2. Ammonium and Sulfate Salts

The issue regarding the surface activity of ions such as halides is gaining importance because of the increasing evidence that surfaces play key roles in heterogeneous atmospheric chemistry.[67,68,81−83] The experimental surface studies and molecular dynamics simulations described above converge to a picture of the larger halide ions (Cl^-, Br^-, and I^-) existing at the air/aqueous interface, a finding which has important ramifications for the reaction of ozone with sea salt aerosols. Sulfate is another anion commonly found in tropospheric and stratospheric aerosols. The concentration of sulfuric acid in tropospheric aerosols is typically greater than 40 wt % and can be neutralized by gaseous ammonia

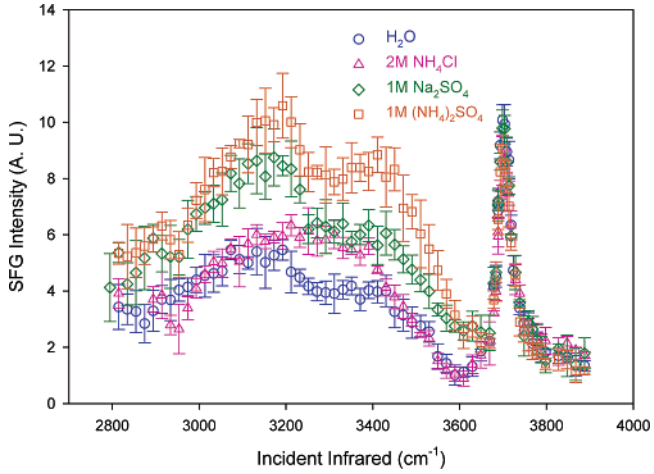

Figure 7. SFG *ssp* polarized spectra of various salt solutions compared to that of neat water. $T \sim 24$ °C (1 M = 0.018*x*, 2 M = 0.036*x*). Reprinted with permission from ref 43. Copyright 2005 American Chemical Society.

to form NH_4HSO_4 and $(NH_4)_2SO_4$.[84] Several studies have shown that ammonium sulfate aerosols are abundant in the atmosphere;[85−88] Talbot *et al*. have measured comparable amounts of NH_4^+ and SO_4^{2-} in tropospheric aerosols.[89] In light of the importance of ammonium sulfate in tropospheric aerosol growth and transformation, the water structure at the air/aqueous interface of aqueous solutions containing NH_4^+ and SO_4^{2-} was studied via SFG spectroscopy and MD simulations,[43] in a vein similar to that described in the study of the sodium halide salts by Liu *et al*.[44]

In the case of the monovalent, atomic halide anions, the surface specificity correlates with the polarizability and size of the anion. The picture gets more complex when molecular and/or multivalent ions are present in aqueous solutions. The divalent sulfate ion is relatively polarizable;[63] however, the energy cost for bringing it close to the air/aqueous surface is high. On the other hand, the ammonium cation is monovalent and polarizable and, thus, more likely to show a propensity to be near the surface, in contrast to the "hard" Na^+ cation.

SFG spectra, *ssp* polarization, of the air/aqueous ammonium sulfate interface are shown in Figure 7. Comparison of the SFG spectra of neat water and aqueous $(NH_4)_2SO_4$ clearly shows different spectral intensities. There is a significant increase in intensity within the hydrogen-bonding region (2800−3600 cm^{-1}) of the aqueous $(NH_4)_2SO_4$ relative to that of neat water. To interpret the SFG spectrum of aqueous $(NH_4)_2SO_4$, a study of aqueous solutions of NH_4Cl and Na_2SO_4 was conducted to determine how individual ions affect the hydrogen-bonding network of water. These spectra are shown in Figure 7 and clearly reveal an intensity enhancement in the OH stretching region (3000−3600 cm^{-1}) in the case of Na_2SO_4 and $(NH_4)_2SO_4$. Comparison of the SFG peak areas for the 3200 and 3450 cm^{-1} peaks with the corresponding Raman times the IR intensities reveals a significant enhancement of both peak intensities at the air/aqueous interface relative to the bulk.

An explanation for the enhancement of the 3200 and 3450 cm^{-1} bands in the SFG spectra could be an increased ordering of the interfacial water molecules under the influence of a local weak electric field induced by the sulfate dianions in aqueous Na_2SO_4 and $(NH_4)_2SO_4$ and/or an increase in the interfacial depth. (Recall that the SFG intensity is proportional to the square of the number density (*N*), as per eq 13,

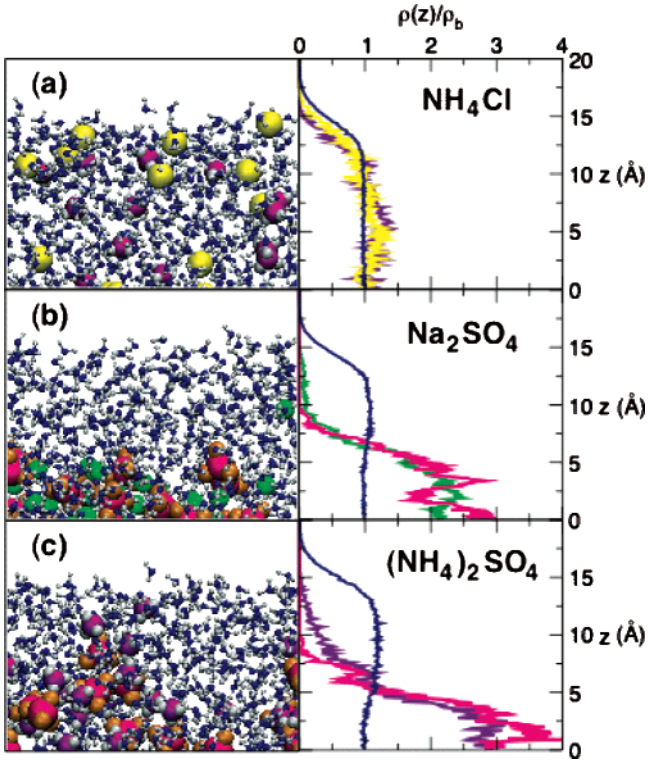

Figure 8. Left panels: snapshots from MD simulations of 0.02*x* (1.2 M) aqueous solutions of (a) ammonium chloride, (b) sodium sulfate, and (c) ammonium sulfate. Right panels: corresponding density profiles of salt ions and water oxygens from the center of the slab ($z = 0$) to the air/water interface. Coloring scheme: H, gray; water O, blue; chloride, yellow; sodium, green; ammonium N, purple; sulfate S, magenta; sulfate O, orange. Reprinted with permission from ref 43. Copyright 2005 American Chemical Society.

and that the intensities from the *ssp* polarized SFG spectra increase if the water molecules are better aligned with their transition moments normal to the surface; yet, cancellation will occur if the vectors oppose each other.) The local weak electric field effect does not include the solvation shell water molecules that partially contribute to the 3450 cm^{-1} band of the salt solutions. However, the local weak electric field does include water molecules beyond the first solvation shell; that is, the local charge of the sulfate dianion has a relatively long-range impact on the orientation of water well beyond the immediate vicinity of the dianion. This effect is borne out in the observed 3200 cm^{-1} band intensity increases of the sulfate solutions. The above explanation of a field effect is also consistent with molecular dynamics simulations on the aqueous solutions of NH_4Cl, Na_2SO_4, and $(NH_4)_2SO_4$ shown in Figure 8.

The thickening of the interface can contribute to the increase in the SFG intensity in the 3200 and the 3450 cm^{-1} regions from the sulfate solutions. It is not possible to distinguish between SFG signal enhancement due to ordering of water molecules under the presence of a weak electrostatic field and an increase in interfacial depth. However, the thickening of the interface is supported by the density profiles from MD simulations[43] (Figure 8b and c) which reveal that the interfacial depth increases in aqueous Na_2SO_4 and $(NH_4)_2SO_4$ (the density gradients extend over a larger region) as compared to aqueous NH_4Cl (Figure 8a). As stated above, the interface is defined by the concentration inhomogeneity of the different species and lacks an inversion center (and is, hence, SFG active), while the bulk is defined as the region

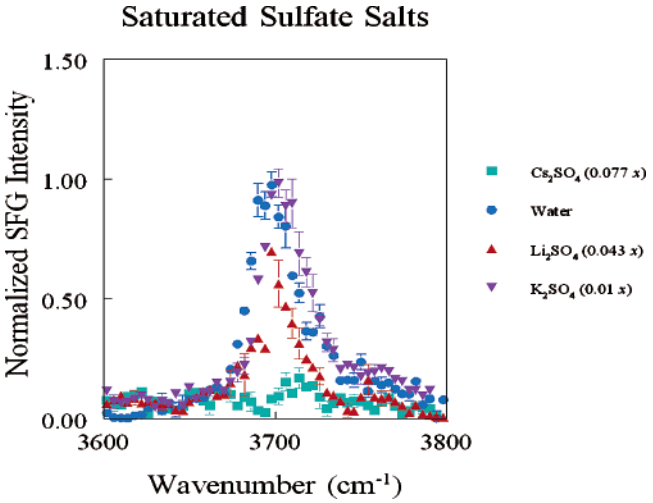

Figure 9. SFG spectrum of saturated sulfate salt solutions: *ssp* polarization, 0 °C.

where the species are homogeneously mixed and, therefore, has a macroscopic center of inversion (and is, hence, SFG inactive). Thus, it is concluded that the air/aqueous interface of the ammonium and sodium sulfate solutions has widened and that local field effects caused by the sulfate dianions play a significant role in this interfacial behavior of water.

3.2.3. Sulfate and Bisulfate Salts

Prior to the groundbreaking work of Shultz and coworkers,[1,42,75,90−93] it was widely believed that small inorganic ions in aqueous solution were located in the bulk and, therefore, do not alter the structure of water at the solution surface. In addition to the experimental measurement of a raised surface tension for ionic salt solutions indicating that the surface is diminished in ion concentration, energetic considerations suggest that charged species have a lower energy when surrounded by complete hydration shells. Thus, it was believed that an SFG spectrum of the surface of an aqueous solution would be identical to that of water.

The issue of the structure of water on the surface is relevant to models for the fate of numerous atmospheric species, many of which depend on the reaction rate at heterogeneous surfaces. In particular, ions at the surface have a significant impact both on heterogeneous reaction mechanisms and on rates.[94−99] Ions in the top monolayer can both orient reacting species and bring reacting partners together in addition to being easily accessible for exchange reactions.

Since the free OH necessarily is located in the top monolayer, we first focus on this region for the sulfate salt solutions. Figure 9 shows the free OH SFG spectrum of several saturated sulfate salt solutions along with that of water for comparison. Note that the saturated concentration is different for the different cations: K_2SO_4 saturates at 0.01*x* while a Cs_2SO_4 solution saturates at a much greater 0.077*x* concentration. The free OH intensity decreases when the salt concentration increases. Since sulfate carries a double charge, and the cations are generally less polarizable than anions, this effect on the top monolayer is unexpected if the salt remains fully ionized and in the bulk.

In aqueous solution, the sulfate anion is in equilibrium with bisulfate and hydroxide. Bisulfate is less highly charged than sulfate; hence, bisulfate is energetically less unfavorable at the surface layer. The general result of negative interfacial ions is demonstrated by the halide ion series results.[6,44,76]

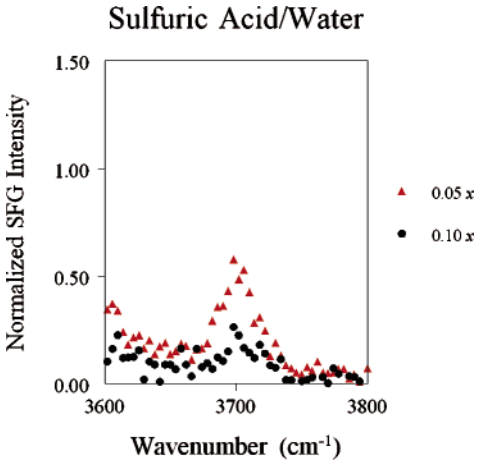

Figure 10. SFG spectrum of the free OH region of sulfuric acid solutions: *ssp* polarization, $T = 0$ °C.

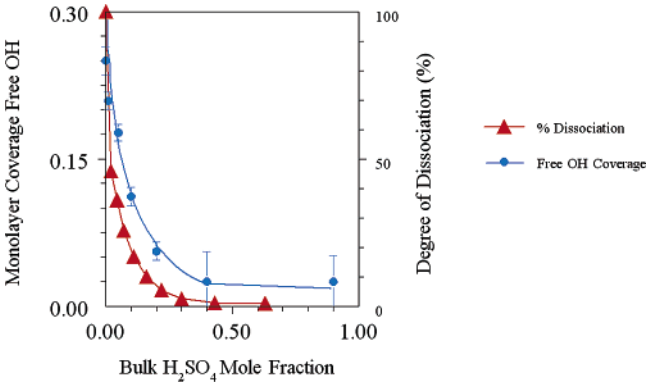

Figure 11. Correlation between the fractional monolayer coverage of free OH and the degree of dissociation for sulfuric acid. Reprinted with permission from ref 22. Copyright 2002 American Chemical Society.

Negative ions result in an enhancement of the 3450 cm^{-1} peak of the water spectrum. However, neither the saturated sulfate salt solutions discussed here nor the lower concentration bisulfate salt solutions (discussed below) show such an enhancement.

A model that fits the sulfate salt solution data, as well as that of sulfuric acid (Figure 10), is that ions form an associated ion pair.[100−105] Energetically, this neutral pair can be found in the interfacial layer, where the pair displaces water from the top monolayer. In the sulfate salts, the free OH diminishes as the salt concentration increases, supporting the model of associated ion pairs. For sulfuric acid, the decrease of the free OH resonance intensity correlates with the degree of association (Figure 11).

The molecular dynamics simulations, shown in Figure 8, indicate that the halide anion distribution has a noticeable dependence on the identity of the associated cation. There is evidence of a similar dependence for the bisulfate salts. Figure 12 shows the free OH region for a 0.01*x* solution of bisulfate salts with the cations Li^+, K^+, and Cs^+ as well as the free OH region of water for comparison. At 0.01*x*, the $LiHSO_4$ solution shows nearly the same intensity as neat water. In contrast, $KHSO_4$ and $CsHSO_4$ both show a diminishment of about half corresponding to a decrease of free OH density on the surface of about 30% (recall that SFG intensity is proportional to the square of the number of scatters). The lithium cation is about half the radius of either potassium or cesium (76 pm compared with 138 and 137

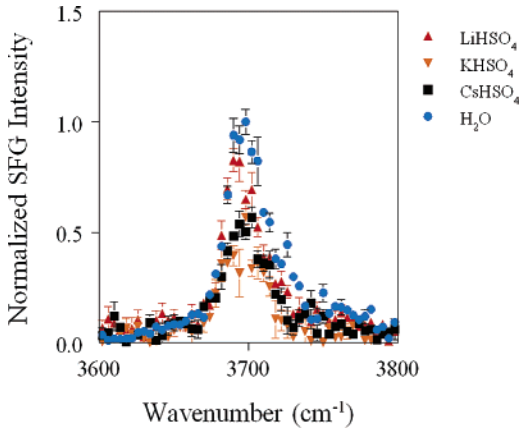

Figure 12. Free OH resonance for a 0.01*x* aqueous solution of the bisulfate salts of Li^+ (up triangles), K^+ (down triangles), and Cs^+. The free OH region of water (circles) is shown for comparison. *ssp* polarization, $T = 0$ °C.

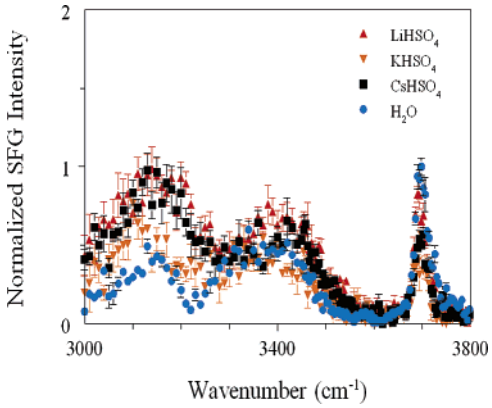

Figure 13. Changes in the SFG spectrum of water upon addition of the salt $LiHSO_4$, $KHSO_4$, or $CsSO_4$. The spectrum of water is shown for comparison. All spectra are with *ssp* polarization and taken at 0 °C.

pm, respectively). It is also less polarizable and, thus, more energetically unfavorable to be found at the surface. It is reasonable that the bisulfate ion distribution also slides more toward the interior when paired with Li^+ than it does when paired with K^+ or Cs^+.

As with the sulfate salts, the 3450 cm^{-1} peak for the bisulfate salts is essentially unaltered from that of water (Figure 13). The 3200 cm^{-1} peak, however, shows a significant enhancement for both $CsHSO_4$ and $LiHSO_4$. In the absence of a definitive assignment of this feature, a clear interpretation of this enhanced intensity is problematic. However, we note that Li^+ is a small ion; hence, the $LiHSO_4$ solution is acidic. As discussed in the following section, H_3O^+ has a propensity to partition to the top monolayer and this location results in an enhancement of the intensity in the 3200 cm^{-1} peak. Both K^+ and Cs^+ are larger ions, so the solutions of $KHSO_4$ and $CsHSO_4$ are both neutral. The enhanced intensity for $CsHSO_4$ must, therefore, have another origin. A more detailed understanding of the ion distributions is needed for a definitive assignment.

3.3. Acids

The effect of acids on the interfacial structure of water is a more complex issue than that of the salts. The cations in aqueous solutions of acids are hydrated proton species such as H_3O^+, $H_5O_2^+$ (Zundel structure), and $H_9O_4^+$ (Eigen

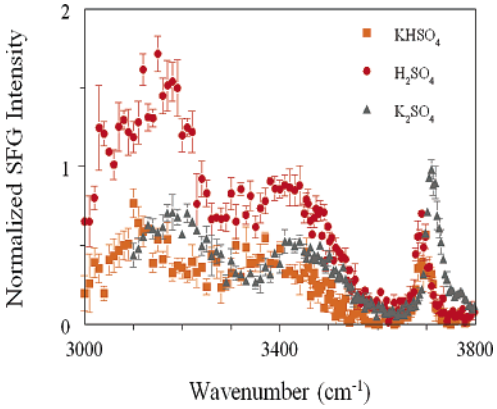

Figure 14. Comparison of the SFG spectrum of the acid H_2SO_4 with those of the salts $KHSO_4$ and K_2SO_4. All concentrations are 0.01*x*, the polarization is *ssp*, and the temperature is 0 °C.

structure),[106] and these species have been credited with giving rise to broad features in the infrared spectra of acids.[107] Moreover, since the proton can hop between water molecules, it is difficult to model the air/aqueous interface of solutions containing these species. A difference between salts and acids, which has been known for a long time, is their effect on the surface tension of water. Whereas salts increase the surface tension of water, it was observed that adding appreciable quantities of monovalent inorganic acids decreases it.[108,109] This implies, via the Gibbs adsorption equation, that there is a net positive surface excess of the acids. Sulfuric acid solutions, like bisulfate solutions, are even more complex. For sulfuric acid, the surface tension initially increases in the low concentration regime and then decreases as one approaches the more concentrated regime.

The first investigation of the aqueous acid/air interface was conducted simultaneously by Shultz[93,110] and Shen.[111] Figure 14 shows a typical spectrum for 0.01*x* H_2SO_4. The major striking feature of the spectrum is the nearly doubled intensity of the 3200 cm^{-1} band. Other acids also show this enhanced intensity[6,42,92,112] but not as dramatically as H_2SO_4 (compare Figure 14 with Figure 15). A recent study by Mucha *et al.*, coupling experimental SFG studies with MD simulations for aqueous solutions of the halogen acids, HCl, HBr, and HI,[6] shows an enhancement of the 3200 cm^{-1} region with a smaller change in the 3450 cm^{-1} peak (Figure 15), consistent with the studies of Radüge *et al.*,[111] Baldelli *et al.*,[92,93,110] and Schnitzer *et al.*[42] It is clear that the hydrated proton affects the structure of the surface of water differently than do other cations.

At higher concentrations, a decrease in intensity in the dangling OH stretch at 3700 cm^{-1} is also observed in all the acids. This decrease may be due to ions or associated ions displacing surface water, or to reorientation tying up the dangling OH groups, or to a combination of the two. Distinguishing between these sources awaits further experimental and theoretical work.

Interpretation of the increased intensity in the 3200 cm^{-1} region is less straightforward than that of the diminished free OH peak intensity. Due to the lack of theoretical studies on the acid air/aqueous system, the interpretations of the SFG spectra differ. Two interpretations are given here. One interpretation attributes the enhanced SFG intensity at 3200 cm^{-1} to a combination of two factors, the hydronium cations in the interfacial region and an increase in interfacial depth, i.e., probing more water molecules.[6] An alternate interpretation attributes the enhanced 3200 cm^{-1} intensity to an

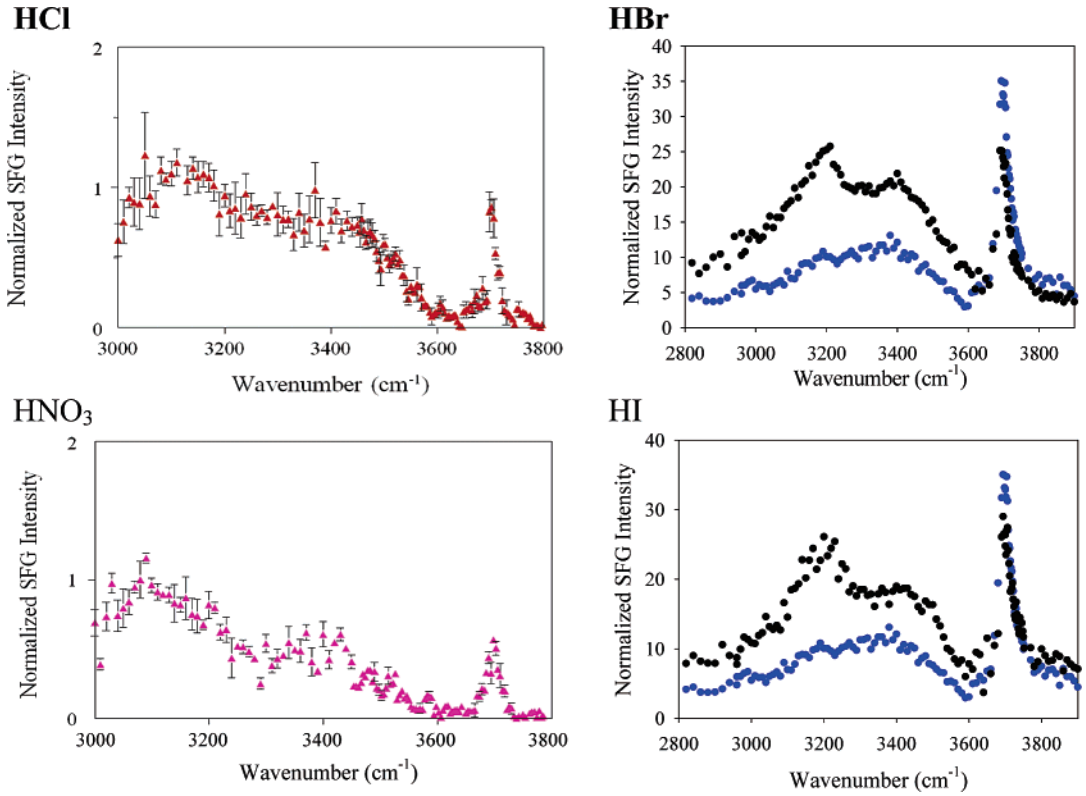

Figure 15. SFG spectra of 0.01*x* acids: *ssp* polarization. HCl and HNO_3 spectra ($T = 0$ °C) are normalized and referenced to the free OH peak of water, and HBr and HI spectra ($T = 24$ °C) are normalized to IR intensity. HCl spectrum reprinted with permission from ref 92, Copyright 1999 Elsevier. HNO_3 spectrum reprinted with permission from ref 42, Copyright 1999 American Chemical Society. HBr and HI spectra reprinted with permission from ref 6, Copyright 2005 American Chemical Society.

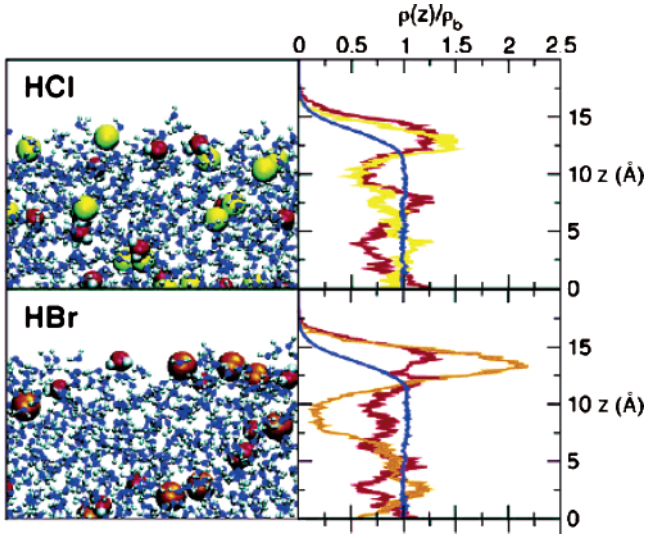

Figure 16. Snapshots from molecular dynamics simulations and density profiles for 0.01*x* aqueous HCl and HBr. Coloring scheme: water oxygen, blue; hydronium oxygen, red; hydrogen, gray; chloride ions, yellow; bromide ions, orange. Reprinted with permission from ref 6. Copyright 2005 American Chemical Society.

interfacial potential due to the ion distribution resulting in a slight reorientation of interfacial water molecules resulting in an increased projection of the transition dipole onto the surface normal. Each of these is discussed in the following paragraphs.

In evaluation of Raman and infrared spectra of aqueous acid bulk solutions, it is apparent that there is an intensity increase that affects a broad spectral region, which extends beyond 3000 cm^{-1}. This intensity increase in Raman and infrared spectra has been referred to as a proton continuum.[107] Since SFG intensity is proportional to Raman and infrared intensities, an enhanced SFG response is expected if the acid is part of the interface. (Recall that the interface is defined as the region of density change between the air and bulk liquid phases.) Since the acid, cations, and anions are indeed part of the interfacial region, a portion of the intense, 3200 cm^{-1} SFG signal observed from the acid solutions is likely due to H_3O^+.

For the halide acids, both the hydronium cations and the anions exhibit a propensity for the air/solution interface as shown in Figure 16.While the affinity of H_3O^+ for the surface is relatively weak, anions exhibit specificity that correlates with the ion polarizability and size. Br^- and I^- (as well as, e.g., N_3^- or NO_3^-)[113−115] show a stronger surface enhancement, while the surface propensity of Cl^- is comparable to that of H_3O^+. As a result of the surface propensity of both cations and anions in aqueous HCl, HBr, or HI, there is a net positive surface excess of ions. In the corresponding salt solutions, the cations, which are small and relatively nonpolarizable spherical ions, are repelled from the surface. In the salt solutions, the anions exhibit ion-specific degrees of surface enhancement slightly less than those in the cases of the corresponding acids. The result of strong cationic repulsion and varying anionic surface propensity is a net depletion of ions from the interfacial layer of aqueous salt solutions. This is very different than results from acids.

An alternate model for the 3200 cm^{-1} enhancement in the SFG spectra of the acids is based on surface potential. That is, the ion distribution at the interface gives rise to a surface potential that has a long-range effect on the orientation of water molecules in the interfacial region.[116] SFG spectroscopy of eicosanoic acid by Gurau *et al.*[116] indicates that water molecules solvating the headgroup result in the 3450 cm^{-1} band dominating the spectrum. However, when a divalent cation (Zn^{2+}) coordinates the headgroups, thus displacing water, there is little intensity in the 3450 cm^{-1} peak. Intensity in the 3200 cm^{-1} peak is unaffected by displacement of water, leading to the conclusion that the 3200 cm^{-1} peak results from water in subsequent layers. The intensity in the 3200 cm^{-1} band is proportional to the interfacial potential which affects the orientation of water molecules in subsequent layers.

Additional evidence that supports the surface potential argument for the 3200 cm^{-1} band in the SFG spectra of the acids comes from recent work by Shen and co-workers.[31] These researchers have used a novel phase-sensitive spectroscopy to determine the orientation of water molecules at a hydrophilic quartz surface as a function of pH. This spectroscopy exploits the phase sensitivity of SFG by using a single-crystal quartz substrate as a reference. The first use of quartz as a reference to determine the absolute orientation of interfacial molecules involved determination of the orientation of phenol, *p*-nitrophenol, *p*-bromophenol, and, most importantly, water, all at the air/water interfaces.[32] In the recent work,[31] use of the single-crystal reference exploits the 3-fold symmetry of the quartz crystal**,** which results in a zero nonresonant signal at ±30° from the symmetry axis. Rotation by 30° ± γ introduces a nonresonant signal with ± phase. This reference phase enables determination of the orientation of water molecules with respect to the surface. The intensity of the 3200 cm^{-1} peak changes with pH and is found to decompose into two peaks: one is centered at 3000 cm^{-1}, has oxygen facing the interface, and has a nearly constant intensity to about pH = 8 which then decreases with increasing pH; the other at 3200 cm^{-1} has the hydrogen atoms facing the interface and has low intensity to pH = 5 which then increases with increasing pH. At high pH, the quartz surface is negatively charged and the SFG intensity is much greater than that at low pH. The 3450 cm^{-1} band has hydrogen facing the interface at all pH values**,** increases intensity to pH ∼ 4.5, and remains relatively constant as pH increases further. None of these resonances in the 3000−3800 cm^{-1} range is readily attributed to hydrated proton species.

To double the intensity in the 3200 cm^{-1} region, the number of oscillators contributing to this resonance need only increase by a factor of 1.4 (the SFG intensity is proportional to the square of the number of oscillators) or the average orientation of these dipoles need change by only 2°. (The 2° estimate is based on the known average orientation of the water dipole at −5° from the surface normal.) Penetration of a given ion to the interface, e.g. Cl^-, is dependent on the counterion (Figure 8 and Figure 1 of ref 6); that is, at 1.2 M, the ion distributions are correlated. The intensity of the 3200 cm^{-1} peak depends on the potential developed due to differences in these distributions. In the acids, the presence of the hydronium ion near the top monolayer enhances the potential. This potential enhancement is particularly pronounced for sulfuric acid since it is a diprotic acid and the SO_4^{2-} anion carries a double charge and, hence, is located deeper within the subsurface.

The intensity of the 3450 cm^{-1} band, which is assigned to oscillating dipoles about the tetracoordinated interfacial water molecules in these acid solutions, shows a varied response. The 3450 cm^{-1} band increases relative to neat

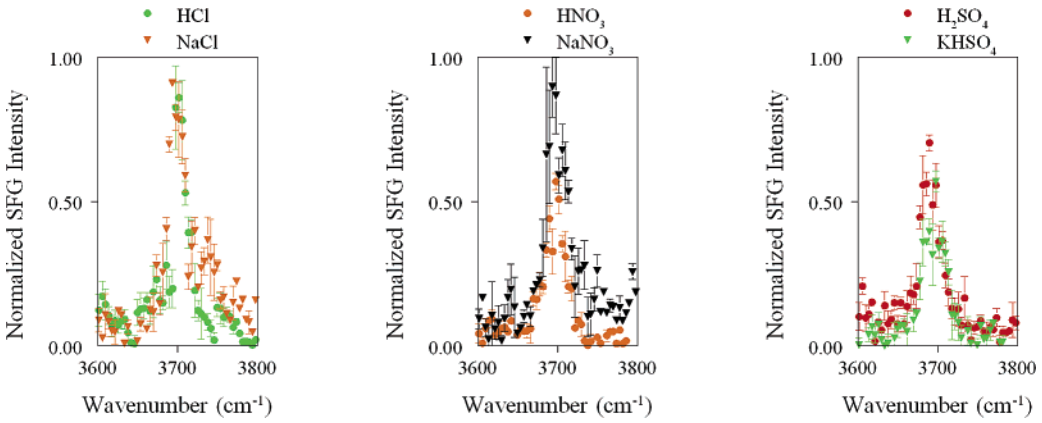

Figure 17. SFG spectra of the free OH region for acids (triangles) compared with the corresponding sodium or potassium salts (circles). Polarization: *ssp*. $T = 0$ °C. Concentration: $0.01x$ (0.56 M).

water for $I^- \sim Br^- > Cl^-$ acids, though to a lesser extent than the 3200 cm^{-1} band. The intensity increase was interpreted as a combination of interfacial depth and an increased surface activity of the acid hydronium and anion by Allen and co-workers.[6]

In the 3700 cm^{-1} region, the sharp peak assigned to the dangling OH of water molecules that straddle the air/solution interface decreases for the higher concentration acids (see Figures 14 and 15) relative to neat water, although there is a small increase on the higher energy side next to this peak for the halogen acids. At low concentration, $0.01x$, all the acids except HCl have a diminished free OH intensity. Since the free OH necessarily is due to water molecules in the very top monolayer, reduction in this intensity indicates that the influence of the acid reaches to the very top layer of the solution. As concentration increases, the free OH intensity decreases yet further.[112] Both molecular dynamics and SFG studies have been done for the $0.015x$ (1.2 M) solution, and a calculation for HBr serves to illustrate the effect of the interfacial ions. The interfacial Br^- ion concentration is double that of the bulk while H_3O^+ shows a smaller enhancement. Thus, the surface ion concentration is $\sim 0.044x$. It has been estimated that the free OH accounts for $0.2x$ of the surface water molecules.[16] If the Br^- ions randomly displace water, the free OH population would be reduced by $0.009x$. Since the SFG signal is proportional to the square of the number of signal generators, the result would be a reduction of the SFG signal to ~91% of the unperturbed intensity. Experimentally, the signal intensity is reduced to about 75% of that for neat water. Thus, the ions in the interface must alter the orientation of water molecules in the top monolayer. Deconvoluting reorientation and displacement to develop a quantitative model of the interface awaits further theoretical and experimental developments.

In summary, there are several interpretations of the factors that may contribute to the 3200 cm^{-1} intensity increase and free OH intensity decrease observed in SFG spectra of acids. Distinguishing among the partitioning of H_3O^+, interfacial depth, and surface potential awaits further experimental and theoretical results.

3.4. Acids versus Salts

In light of the preceding discussion of acids and salts, it is instructive to compare the two. The choice of anion for the salt is important here: It should be neither surface active nor so small that cation hydration results in a significantly acidic solution. Both Na^+ and K^+ meet these criteria. This choice is verified by comparing the SFG spectra of NaCl and KCl with that of water: they are indistinguishable.

Figure 17 shows the free OH regions for HCl compared with NaCl, HNO_3 compared with $NaNO_3$, and H_2SO_4 compared with $KHSO_4$. Since the salt cation does not affect surface water, the free OH region of the salt reflects perturbation of the top monolayer by the anion, possibly modified by the anion carrying the cation to the interface. Similarly, comparison of the acid to the salt reflects the direct effect of H_3O^+ (and other proton hydrates) plus the influence of the hydrated proton on the anion distribution.

As previously noted, NaCl does not affect the structure of the free OH. The nitrate anion appears to be similar to the chloride anion in this regard: at $0.01x$ the spectrum of the aqueous $NaNO_3$ surface is indistinguishable from that of water. The bisulfate anion, however, results in reduction of the free OH resonance. The bisulfate anion either penetrates to the top monolayer displacing water or penetrates close enough that the Coulombic field results in a reorientation of surface water molecules suppressing the resonance intensity. If the bisulfate anion simply displaces water, it must displace 25% of the water to result in the observed intensity decrease. With a 1% bulk concentration, this implies an impressive surface enhancement. It is probably more likely that the negative Coulombic field of the anion results in fewer dangling OH groups; however, this conclusion requires further exploration.

Comparing the acids to their respective salts indicates that HCl and H_2SO_4 have a similar effect on surface water as do their salts at a concentration of $0.01x$. In contrast, HNO_3 shows about a 40% decrease in intensity compared with its salt. This suggests that nitrate more readily forms a contact ion pair with the hydrated proton than do either chloride or bisulfate. This conclusion is supported by a wider view of the hydrogen-bonded region of water discussed in the next paragraphs.

As reiterated above, there is no clear agreement on assignment of the resonances in the hydrogen-bonded region of water. However, the work discussed previously supports an interpretative assignment. Enhancement of the broad peak centered at about 3400−3450 cm^{-1} reflects a short-range polar ordering due to negative ions in the interface. An increased intensity in the broad peak centered at about 3150−3200 cm^{-1} reflects a longer range surface potential that is most pronounced in the presence of hydrated proton species. Figure 18 shows SFG spectra of the OH stretch region of the acids HCl, HNO_3, and H_2SO_4 along with their corre-

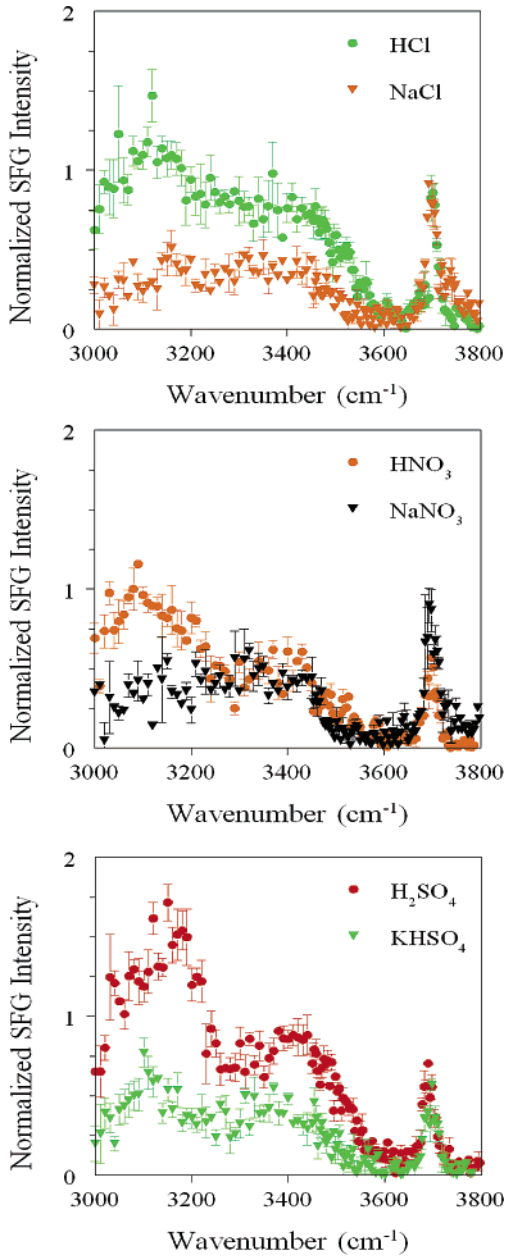

Figure 18. SFG spectra of the OH stretch region for the acids HCl, HNO_3, and H_2SO_4 compared with their corresponding sodium and potassium salts. Polarization: *ssp*. $T = 0$ °C. Concentration: 0.01*x* (0.56 M).

sponding salts. Of the three anions, Cl^- and HSO_4^- result in an enhancement of the 3400−3450 cm^{-1} peak. The dominant role of the halides in influencing the 3450 cm^{-1} band is similar to observations from Raman spectroscopy of the bulk salt solutions[44] and is consistent with short-range order as discussed above. The nitrate anion, even when paired with hydrated proton species, does not enhance this resonance: The proton−nitrate pair is distinctly different from other anion−proton combinations. Since the free OH resonance is diminished with HNO_3, this combination must approach the interface but lack the negative charge required for enhancement of the 3400−3450 cm^{-1} resonance. A consistent interpretation is that the ions form a contact ion pair that displaces water in the top monolayer. Enhancement of the 3150−3200 cm^{-1} peak suggests that the orientation of this contact ion pair creates a surface potential similar to that of acids with less correlated proton−anion pairs.

HCl is well-known to ionize on surfaces,[92,117−123] and recent molecular dynamics calculations[77,124,125] indicate that chloride is surface active; it is, therefore, not surprising to see an enhancement of the 3400−3450 cm^{-1} peak for HCl. However, since the free OH peak intensity is unaltered at this concentration, the chloride anion concentration in the top monolayer cannot be enhanced significantly relative to that of the bulk. Similarly, the hydrated proton species concentration is not enhanced relative to that of the bulk. The combination is not so surprising considering the volatility of HCl: Any contact ion pair found in the top monolayer simply departs to the gas phase. Note that, at higher HCl concentrations, the free OH peak intensity is observed to decrease.[6,42,92,112]

Compared with HCl, H_2SO_4 is much less volatile. Either separate or contact ions remain in the interface. The separate and contact ions suppress the free OH intensity, the anions impart short-range order enhancing the 3400−3450 cm^{-1} band, and the combination of hydrated protons and bisulfate/sulfate anions gives rise to a surface potential that results in the largest enhancement of the 3150−3200 cm^{-1} band of all acids and salts investigated to date.

In summary, the effect of salts and acids on the aqueous interface is generally complex. Either ions or contact ion pairs in the top monolayer suppress dangling OH groups, negative ions in the interface result in short-range order and enhancement of the 3400−3450 cm^{-1} peak, and the combination of the distribution of hydrated protons and associated anions can give rise to a surface potential that increases the intensity of the 3150−3200 cm^{-1} band. The 3200 cm^{-1} band (in many cases, closer to 3100 cm^{-1}) increases coupled with the dangling OH (3700 cm^{-1}) peak decreases are unique to the acids and are not observed for the sodium salt air/solution interfaces.

While a picture of the nature of aqueous solution interfaces is beginning to emerge, it is apparent that further experiments and theoretical developments are needed before the picture is made clear.

3.5. Cluster Studies on Protonated Water

Cluster calculations are enormously helpful for understanding the possible structures of the hydrated proton at the interface.[113,126,127] On average, water molecules in bulk water are four coordinate. At the surface, there is necessarily an unsatisfied coordination. In contrast, the coordination number for the hydrated proton is smaller due to the poor proton acceptor ability of the hydronium oxygen (formally, the oxygen carries the positive charge). As a result, the coordination number of the hydronium ion—the number of water molecules in the first hydration shell of the hydronium ion—is 3.6.[128] This lower coordination stabilizes the hydronium ion at the interface relative to the bulk and leads to the recently recognized surface activity.[6] Mass spectrometry results for protonated clusters find an unusual stability for the $(H_2O)_{21}H^+$ cluster,[129] which consists of a cage with a single interior molecule. Calculations[127] indicate that the proton is on the exterior of this cage with no low-lying structures containing an interior H_3O^+.

The vibrational signature of hydrated proton clusters has been investigated by the infrared photoionization action spectrum of size-selected, $(H_2O)_nH^+$ clusters.[57] Clusters with *n* larger than 8 show a broad, intense band centered at 3450 cm^{-1}. The main dangling OH peak appears at 3700 cm^{-1} and is relatively sharp. A smaller, sharp feature appears at

3720 cm^{-1} for clusters of 18−20 water molecules. This feature disappears at $n = 21$, reappears at $n = 23$, and persists for yet larger clusters. The doublet at 3700 and 3720 cm^{-1} is due to two types of free OH: those associated with DAA water and those associated with DA water. The $n = 21$ and 22 clusters have a dodecahedral structure with a water molecule inside the cage. The proton on the surface is in an Eigen structure with three waters hydrating the proton.

James and Wales[127] use an empirical valence bond potential to examine the effect of increasing temperature on the structure of protonated water clusters. As temperature increases, the stable structure converts from ring structures to treelike structures. A mixture of two- and three-coordinate water molecules results in a doublet in the dangling OH region while closed cages have three-coordinate water molecules and a single dangling OH peak.

The theoretical results[6,57] give a consistent picture for the dangling OH region for acidic solutions. The concentration of the hydrated proton is enhanced on the surface. Water molecules hydrating the proton consisting of three-coordinate molecules give rise to a single dangling OH peak at 3700 cm^{-1}, while the presence of two-coordinate water molecules gives rise to a second peak at 3720 cm^{-1}. The picture for the hydrogen-bonded region, in particular the band at 3200 cm^{-1}, is less definitive. Protonated cluster spectroscopy shows a broad infrared band in the 3450 cm^{-1} region but little intensity in the 3200 cm^{-1} region.[57] It is clear that the hydrated proton is at the surface. Unraveling the effect on the hydrogen-bonded region awaits studies on larger clusters.

3.6. Ammonia

Ammonia−water solutions are of importance to numerous areas of chemistry from agriculture, to living organisms, to detergents and industrial processes. As the dominant, soluble basic gas in the atmosphere (0.1−10 ppb), ammonia reacts with acidic solutions to form particulate matter that serves as cloud condensation nuclei.[130]

Due to the importance of ammonia, the structure of the ammonia solution/air interface is of interest in its own right. In addition, ammonia solutions are of interest here both for what they reveal about the structure of water at the interface and for the clustering model that they suggest for transport across the aqueous/air interface. (The clustering model is discussed below.)

As early as 1928, Rice[131] proposed that aqueous ammonia solutions feature an ammonia−water complex on the interface. However, the nature and existence of this complex remained unexplored until application of surface-sensitive vibrational spectroscopy[132,133] and uptake measurements[134,135] revealed the presence of this complex. Figure 19 shows the SFG spectrum of the aqueous ammonia interface. The sharp feature at 3333 cm^{-1} in the gas-phase spectrum is the NH_3 symmetric stretch. Oriented nearly vertically relative to the surface plane,[133] the symmetric stretch is the most prominent feature of the surface spectrum. Note that the symmetric stretch is shifted by only about 20 cm^{-1} upon attachment to the surface, indicating a weak interaction between ammonia and water.

Both SFG and uptake model-calculated surface coverage indicate that the surface ammonia concentration is considerably larger than the surface excess calculated from surface tension data. (A larger surface excess has also been noted for glycerol−water solutions[136] and is attributed to the deeper interfacial layer probed by surface tension compared with

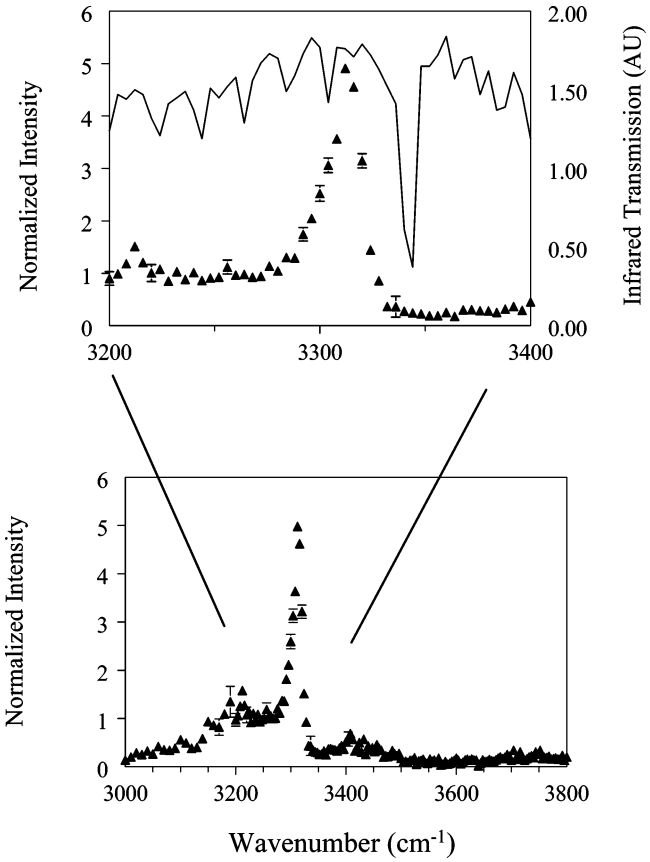

Figure 19. SFG spectrum with *ssp* polarization (▲) compared with the gas-phase absorption (—) obtained simultaneously through the headspace port. The lower panel is a survey of the 3000−3800 cm^{-1} region. $T = 0$ °C. Reprinted with permission from ref 22. Copyright 2002 American Chemical Society.

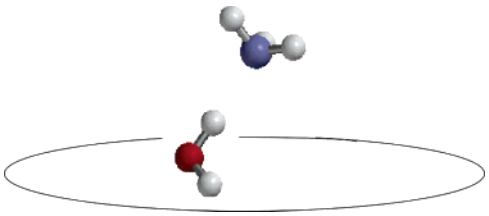

Figure 20. Cartoon of ammonia docking onto the free OH group of water at the interface.

SFG.) The saturation coverage for ammonia on water is (1.2 ± 0.2) × 10^{14} molecules/cm,[2,137] close to the estimated surface coverage of 2 × 10^{14} molecules/cm^2 for free OH groups on neat water.[16] This suggests that, at saturation, ammonia simply caps the dangling OH groups at the surface of a truncated solution, making surface water molecules four-coordinate (Figure 20). Since ammonia is a weak hydrogen bond donor, the three hydrogen atoms face the vapor side of the interface. Indeed, SFG measurements reveal that the ammonia C_3 axis is tilted off the surface normal by 25−38°,[133] an angle consistent with that of the dangling OH for molecules straddling the interface.

Transport across the interface involves a progression from a surface adsorbed species into a fully solvated solute, which is accommodated into the bulk. Accommodation is described by a mass accommodation coefficient, α. If there is no barrier to accommodation, $\alpha = 1$. Experimental observations that α is less than one and that ΔH_{obs} and ΔS_{obs} are correlated, as is the case for ammonia, support a model suggesting a critical cluster size in the surface region in order for

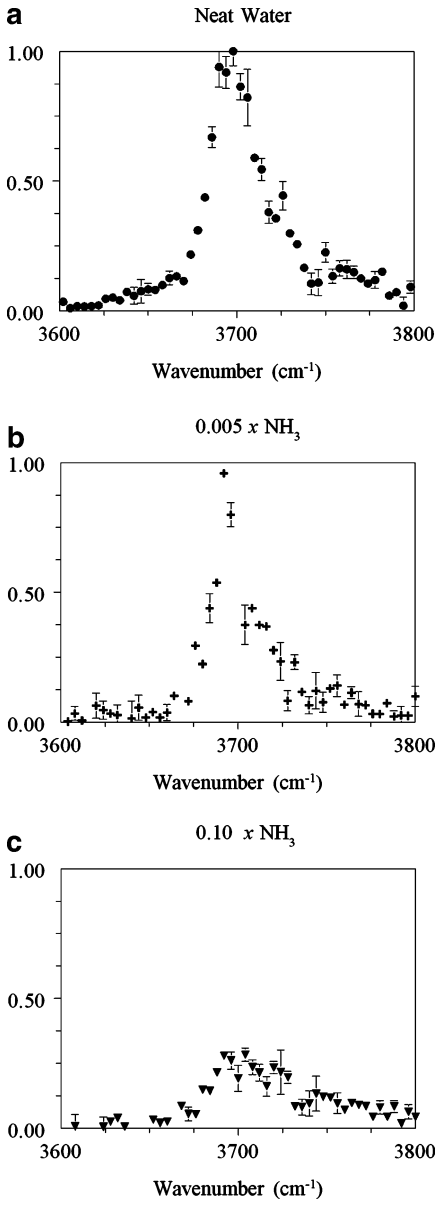

Figure 21. Magnification of the free OH region for ammonia solutions: *ssp* polarization, 0 °C. Reprinted with permission from ref 22. Copyright 2002 American Chemical Society.

accommodation to occur.[137,138] That is, an ammonia molecule enters the narrow surface region of dense gas where nucleation occurs.[138] Upon formation of a critical cluster, ammonia enters the bulk. The critical cluster size is between two and three water molecules.[139] This critical cluster model is consistent with surface reaction models[140] that indicate a free energy profile for approach to and transport across the aqueous interface for ammonia that is very similar to the profile for water. Specifically, there is no barrier for incorporation into the bulk. Thus, the surface excess results not from an energetic barrier to solvation but rather from kinetic generation of the critical cluster.

SFG spectra of the ammonia solution interface also reveal more detail about the free OH region. There has been some speculation, based on spectral fitting, that the free OH peak actually consists of two components.[41] Ammonia−water solutions show this second component (Figure 21) and validate the picture of ammonia docking onto the dangling OH groups. With as little as 0.005*x* NH_3, the free OH peak is considerably narrowed and diminished in intensity (Figure 21b). With $x = 0.05$, there remains a broad peak that persists to nearly $x = 0.20$ (Figure 21c). Cluster studies help provide insight into the possible origin of this broad feature.

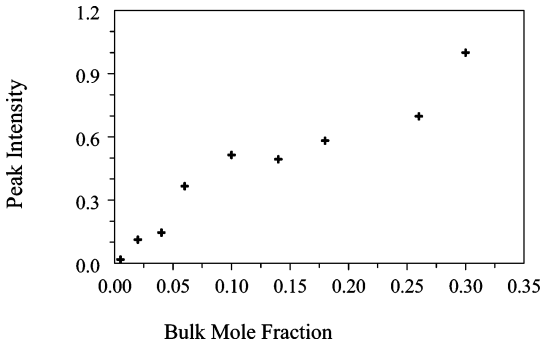

Figure 22. SFG intensity for the symmetric stretch of ammonia as a function of bulk mole fraction. Polarization is *ssp*. $T = 0$ °C. Reprinted with permission from ref 22. Copyright 2002 American Chemical Society.

In larger clusters, i.e., $(H_2O)_n$ where $n > 18$ (other than $n = 21$), there is a doublet in the free OH region: one peak at 3700 cm^{-1} and a second at 3720 cm^{-1}.[57] The former is assigned to DAA water, and the latter to DA water. Incorporation of ammonia into the surface "lattice" may well weaken the hydrogen bonding of a dangling OH water molecule in the vicinity, weakening hydrogen bonding of that water to its neighbors and moving the free OH stretch to nearer the gas-phase antisymmetric stretch. This also explains the very broad nature of this feature. Correlation of the broad feature intensity with the surface ammonia concentration compared with the bulk concentration helps support this picture of the feature's origin.

Tracking the surface ammonia concentration as a function of the bulk concentration reveals three concentration regions (Figure 22). At low concentration, ammonia simply titrates the dangling OH, with the free OH intensity decreasing in tandem with the ammonia intensity increase. In the middle concentration range, the surface ammonia concentration remains essentially constant while the bulk concentration increases from $x = 0.1$ to more than 0.2. Finally, at higher concentration, the ammonia signal increases as the surface becomes crowded with ammonia. The broad, free OH feature of water disappears only when the bulk is fully saturated with ammonia ($x \sim 0.33$). *Ab initio* calculations of the structure of ammonia−water clusters indicate what the surface complex might look like. The $NH_3 \cdot 2H_2O$ has a cyclic structure.[137,141] Directly relevant to the surface, Bacelo[141] examined clusters with three and four water molecules. Embedding the lowest energy clusters into the surface, with ammonia toward the vapor phase, shows water molecules with dangling OH bonds that are near the surface plane and, thus, less accessible for hydrogen bonding to additional ammonia molecules.

In summary, the ammonia experiments support a picture of the dangling OH groups dividing into two subgroups. One group is easily accessible to impinging gas-phase molecules. The second group is less accessible, giving rise to a broad resonance blue-shifted from the main free OH resonance at 3700 cm^{-1}.

3.7. Nanodrops

Water clusters[49,50,142−144] and water in confined geometry[145] have received increasing attention in recent years due to improved techniques for treating hydrogen-bonded systems

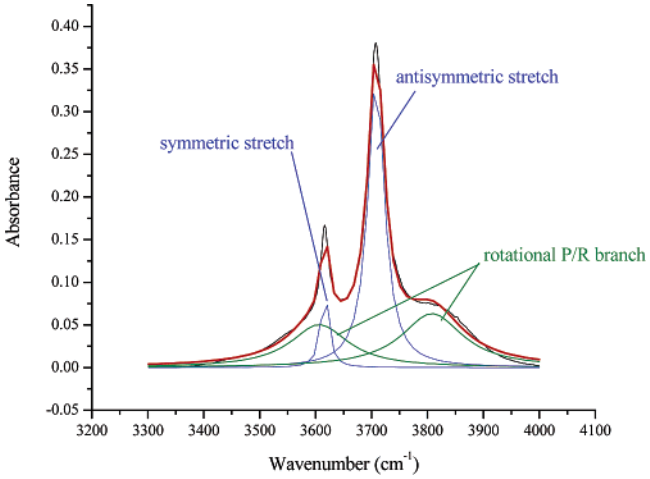

Figure 23. Infrared spectrum of room-temperature CCl_4 saturated with water.

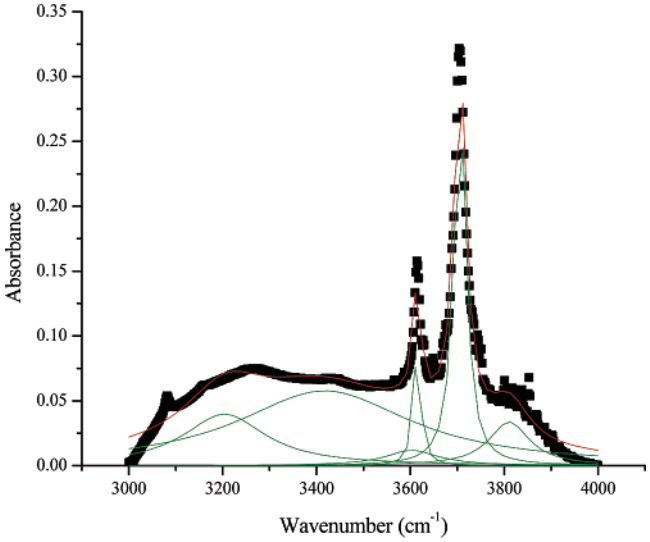

Figure 24. Infrared spectrum of water in CCl_4 cooled to just below 0 °C, illustrating formation of clusters at lower temperature.

both experimentally and theoretically. These cluster studies provide guidance and support for interpreting the aqueous surface spectra discussed in this review. In addition, Shultz and co-workers (unpublished work) have generated near-room-temperature water nanoclusters in a hydrophobic solvent to probe the infrared spectroscopy of dynamically interchanging structures. The solvent for these studies is CCl_4. CCl_4 is an excellent solvent for these studies since the solubility of water is low, on the order of tens of millimolar. Previous studies of this system[146−148] have reported conflicting spectra. The MD simulation of Danten *et al.*[146] indicates water monomers showing a symmetric and antisymmetric stretch as well as rotational sidebands on the antisymmetric stretch. While the infrared spectra of Köddermann[147] and the older work of Magnusson[148] show intensity in the hydrogen-bonded region, Ködderman also resolves a peak on the blue side of the antisymmetric stretch which is attributed to a librational motion of water. The discrepancy appears to be due to hydrogen bonding of water to the window material of the infrared cell.

The issue of hydrogen bonding to the window material can be circumvented by silanizing the IR quartz windows. As shown in Figure 23, only water monomers are present if the window material is silanized. Note, in particular, the absence of any hydrogen-bonded features. The spectrum is well fit by a combination of four Lorentzian lines: the two centered at 3616 and 3708 cm^{-1} are attributed to the symmetric and antisymmetric stretch modes, respectively. (The red-shift compared with the gas-phase spectrum is due to the dielectric constant of the solvent, 2.2379.) The remaining two peaks centered at 3605 and 3805 cm^{-1} are about 130 cm^{-1} wide and symmetrically distributed around the antisymmetric stretch. These broad peaks have the appearance of rotational R and P branches, respectively. (The rotation will be discussed further below.)

Cluster studies[142] suggest an alternate interpretation of the spectrum in Figure 23, namely a water dimer. The free OH stretch of the water dimer occurs at 3735 cm^{-1}, the antisymmetric stretch of the acceptor at 3745 cm^{-1} (these would not be resolved with the peak width of Figure 23), the bonded OH stretch at 3601 cm^{-1}, and the symmetric stretch of the acceptor at 3660 cm^{-1} with a weak oscillator strength. The result would appear as two peaks at about 3740 and 3600 cm^{-1}. This interpretation conflicts with observation of the rotational sidebands. Rotation of the dimer involves rotation of a massive unit that is inconsistent with the broad envelope observed in the spectrum. A librational motion of the acceptor water molecule would give rise to a hot band but not the symmetrically placed bands observed.

Interpretation of the broad peaks as being due to a rotation of a water monomer within the CCl_4 cage is confirmed by deuterium substitution.[149] Upon deuterium substitution, the antisymmetric stretch moves to 2752 cm^{-1} and the broad peaks to 2680 and 2825 cm^{-1}, respectively: a shift toward the vibrational origin of a factor of $1/\sqrt{2}$. The J value for the rotational maximum is proportional to $(kT/B)^{1/2}$, where B is the rotational constant ($=\hbar/4\pi I$) and I is the moment of inertia. The maximum in the rotational envelope is given by the product of the line spacing, $2B$, and the J value of the maximum. The maximum is displaced from the vibrational origin by a shift proportional to $2(BkT)^{1/2} = 2(\hbar kT/4\pi I)^{1/2}$, just as observed for water and heavy water. Symmetry analysis indicates that the rotational motion consists of rotation of the two hydrogen atoms about the oxygen atom in a clockwise or counterclockwise direction, respectively.

Upon cooling the water−CCl_4 solution, a transition to clusters, formation of water nanodrops, occurs. Figure 24 shows a representative spectrum for the solution cooled at slightly below 0 °C. The spectrum contains all the features of the room-temperature spectrum, plus a broad absorbance extending from 3000 cm^{-1} to the monomer features. The broad spectrum is well fit by two broad bands centered at 3200 and 3400 cm^{-1}, respectively. Upon further cooling, the 3400 cm^{-1} peak grows to dominate the spectrum while the 3200 cm^{-1} band remains relatively constant.

A complete interpretation of the cluster spectra awaits further theoretical development. We focus here on aspects of the spectra that help in understanding the SFG spectra of the aqueous interface. The cooled solution contains a broad distribution of cluster sizes with the smallest average size at just below 0 °C. Since no further water is added to the solution, clusters are formed at the expense of water monomers. The broad band at 3805 cm^{-1} has gained intensity relative to both the peak at 3708 cm^{-1} and the band at 3605 cm^{-1}, suggesting a contribution to this intensity in addition to the R rotational branch of the antisymmetric stretch of the monomer. This is suggestive of the high-frequency wing observed for many SFG spectra and shown prominently in

the spectrum of aqueous ammonia from 1 to 20 mol %.[22] For an interpretation of this high-frequency component, we turn to a comparison of the dangling OH frequency for clusters and the prominent SFG peak for the dangling OH on aqueous solutions[16,22,40−42] or ice.[150] Buck[142] points out that the dangling OH peak for clusters is blue-shifted to 3720 cm^{-1} compared with the dominant SFG dangling OH peak at 3695 cm^{-1}. The reasons cited for the blue shift are two: Due to the small number of water molecules in the cluster, the directionality of the hydrogen bond is strained and the neighboring water molecules have a lower coordination than that for bulk surfaces. Calculations for clusters find many 3-fold-coordinate molecules whereas bulk water or ice contains primarily 4-fold-coordinate water among the neighbors. Hence, the 3695 cm^{-1} peak dominates the SFG spectra. The presence of a lower concentration of water molecules with a free OH and strained bonds to low-coordination-number neighbors could account for the additional intensity in the SFG spectra as well as the nanocluster spectra.

As the solution is cooled further, the 3400 cm^{-1} peak grows to dominate the spectrum. It is reasonable to expect that cluster size increases as the temperature is lowered and that the hydrogen-bonded region contains an increasing contribution from four-coordinate versus surface water molecules. Surface molecules are three-coordinate, either DAA or DDA. The dominance of the 3400 cm^{-1} peak at lower temperature supports the assignment of this region to four-coordinate molecules. For SFG, these four-coordinate molecules must be within the surface layer in order to be oriented and contribute to the signal.

For three-coordinate surface molecules, the DAA molecules (the companion to the free OH) have a stronger hydrogen bond and, so, have the largest red shift.[47] This configuration of water molecules will exist whenever a nanocluster forms. Interpretation of the 3200 cm^{-1} peak as being due to the H-bonded stretch of these DAA molecules is consistent with the 3200 cm^{-1} peak developing at just under the clustering temperature.

4. Conclusions and Summary

Spectroscopic studies of surface water structure as it is affected by salts, acids, and ammonia have been presented in this review. Clearly, the interfacial structure of water is highly sensitive to the addition of ionic inorganic solutes. Interfacial water rearranges and restructures. The effects of monovalent inorganic anions depend on the polarizability of the ion, which is related to ion size: the more polarizable the anion, the stronger the effect. In the cases presented here, the interfacial concentration gradients give rise to an increasing interfacial depth. For a divalent inorganic anion, sulfate, interfacial depth also increases. However, the larger charge on the polarizable sulfate anion drives an ordering of the water molecules well beyond the immediate solvation shell. For the corresponding acids, more dramatic affects are observed for the dangling OH, as well as possible surface potential effects. The surface potential and interfacial depth increase due to concentration gradients extending deeper into what was the bulk solution. Protonated water may also be observed. Ammonia, unique in itself, causes changes in the dangling OH. Dangling OH changes are not observed with ammonia's conjugate acid, ammonium. Cluster and aqueous nanodrop studies have significantly contributed to unraveling the effect of ions on the surface.

In the past few years, researchers have made great strides toward a clearer understanding of surface and interfacial water structure as presented here. The trends associated with monovalency, divalency, size, and polarizability provide a deeper understanding of the behavior of water at its own surface. Yet, there remains a great need to further elucidate interfacial water restructuring due to ions in order to develop a quantitative and predictive model for the effect of ions on the aqueous interface.

5. Acknowledgments

We acknowledge the many students and postdocs that have contributed to the Shultz and Allen Labs' research as presented here: Steve Baldelli, Cheryl Schnitzer, Danielle Simonelli, Gang Ma, Lori M. Levering, and M. Roxana Sierra Hernandez. We also acknowledge the National Science Foundation (CHE- 0134131, CHE-0089147, ATM-0413893 (H.C.A.); CHE0240172, CHE9208232, CHE-9256871, US EPA R-822453-01-0, PRF-37517-AC5 (M.J.S.)), Research Corporation: Research Innovation Award (RI0768 (H.C.A.)), Tufts University Faculty Research Fund Award, and the Tufts University Center for Environmental Management (M.J.S.) for funding of this research.

6. References

(1) Shultz, M. J.; Schnitzer, C.; Simonelli, D.; Baldelli, S. *Int. Rev. Phys. Chem.* **2000**, *19*, 123.
(2) Eisenthal, K. B. *Chem. Rev.* **1996**, *96*, 1343.
(3) Shen, Y. R. *Annu. Rev. Phys. Chem.* **1989**, *40*, 327.
(4) Gragson, D. E.; Richmond, G. L. *J. Phys. Chem. B* **1998**, *102*, 3847.
(5) Miranda, P. B.; Shen, Y. R. *J. Phys. Chem. B* **1999**, *103*, 3292.
(6) Mucha, M.; Frigato, T.; Levering, L. M.; Allen, H. C.; Tobias, D. J.; Dang, L. X.; Jungwirth, P. *J. Phys Chem.* **2005**, *109*, 7617.
(7) Cappa, C. D.; Smith, J. D.; Wilson, K. R.; Messer, B. M.; Gilles, M. K.; Cohen, R. C.; Saykally, R. J. *J. Phys. Chem. B* **2005**, *109*, 7046.
(8) Petersen, P. B.; Saykally, R. J. *J. Phys. Chem. B* **2005**, *109*, 7976.
(9) Bloembergen, N.; Pershan, P. S. *Phys. Rev.* **1962**, *128*, 606.
(10) Heinz, T. F.; Tom, H. W. K.; Shen, Y. R. *Phys. Rev. A* **1983**, *28*, 1883.
(11) Goh, M. C.; Hicks, J. M.; Kemnitz, K.; Pinto, G. R.; Bhattacharyya, K.; Eisenthal, K. B.; Heinz, T. F. *J. Phys. Chem.* **1988**, *92*, 5074.
(12) Hunt, J. H.; Guyot-Sionnest, P.; Shen, Y. R. *Chem. Phys. Lett.* **1987**, *133*, 189.
(13) Guyot-Sionnest, P.; Superfine, R.; Hunt, J. H.; Shen, Y. R. *Chem. Phys. Lett.* **1988**, *144*, 1.
(14) Harris, A. L.; Chidsey, C. E. D.; Levinos, N. J.; Loiacono, D. N. *Chem. Phys. Lett.* **1987**, *141*, 350.
(15) Superfine, R.; Huang, J. Y.; Shen, Y. R. *Phys. Rev. Lett.* **1991**, *66*, 1066.
(16) Du, Q.; Superfine, R.; Freysz, E.; Shen, Y. R. *Phys. Rev. Lett.* **1993**, *70*, 2313.
(17) Hommel, E. L.; Allen, H. C. *J. Phys. Chem. B* **2003**, *107*, 10823.
(18) Ma, G.; Allen, H. C. *J. Phys. Chem. A* **2003**, *107*, 6343.
(19) Conboy, J. C.; Messmer, M. C.; Richmond, G. L. *J. Phys. Chem.* **1996**, *100*, 7617.
(20) Gragson, D. E.; Richmond, G. L. *J. Chem. Phys.* **1997**, *107*, 9687.
(21) Messmer, M. C.; Conboy, J. C.; Richmond, G. L. *J. Am. Chem. Soc.* **1995**, *117*, 8039.
(22) Shultz, M. J.; Baldelli, S.; Schnitzer, C.; Simonelli, D. *J. Phys. Chem. B* **2002**, *106*, 5315.
(23) Dick, B.; Gierulski, A.; Marowsky, G.; Reider, G. A. *Appl. Phys. B.* **1985**, *38*, 107.
(24) Hirose, C.; Akamatsu, N.; Domen, K. *Appl. Spectrosc.* **1992**, *46*, 1051.
(25) Muenchausen, R. E.; Keller, R. A.; Nogar, N. S. *J. Opt. Soc. Am.* **1987**, *4*, 237.
(26) Akamatsu, N.; Domen, K.; Hirose, C. *Appl. Spectrosc.* **1992**, *46*, 1051.
(27) Moad, A. J.; Simpson, G. J. *J. Phys. Chem. B* **2004**, *108*, 3548.
(28) Moad, A. J.; Simpson, G. J. *J. Phys. Chem. A* **2005**, *109*, 1316.
(29) Superfine, R.; Huang, J. Y.; Shen, Y. R. *Opt. Lett.* **1990**, *15*, 1276.
(30) Superfine, R.; Huang, J. Y.; Shen, Y. R. *Chem. Phys. Lett.* **1990**, *172*, 303.

(31) Ostroverkhov, V.; Waychunas, G. A.; Shen, Y. R. *Phys. Rev. Lett.* **2005**, *94*, 046102.
(32) Kemnitz, K.; Bhattacharyya, K.; Hicks, J. M.; Pinto, G. R.; Eisenthal, K. B.; Heinz, T. F. *Chem. Phys. Lett.* **1986**, *131*, 285.
(33) Becraft, K. A.; Moore, F. G.; Richmond, G. L. *J. Phys. Chem. B* **2003**, *107*, 3675.
(34) Hirose, C.; Akamatsu, N.; Domen, K. *J. Chem. Phys.* **1992**, *96*, 997.
(35) Dick, B. *Chem. Phys.* **1985**, *96*, 199.
(36) Miragliotta, J.; Polizzotti, R. S.; Rabinowitz, P.; Cameron, S. D.; Hall, R. B. *Chem. Phys.* **1990**, *143*, 123.
(37) Ong, T. H.; Davies, P. B. *J. Phys. Chem.* **1993**, *97*, 12047.
(38) Ong, T. H.; Davies, P. B.; Bain, C. D. *Langmuir* **1993**, *9*, 1836.
(39) Harris, A. L.; Rothberg, L.; Dhar, L.; Levinos, N. J.; Dubois, L. H. *J. Chem. Phys.* **1991**, *94*, 2438.
(40) Allen, H. C.; Raymond, E., A.; Richmond, G. L. *Curr. Opin. Colloid Interface Sci.* **2000**, *5*, 74.
(41) Allen, H. C.; Raymond, E. A.; Richmond, G. L. *J. Phys. Chem. A* **2001**, *105*, 1649.
(42) Schnitzer, C.; Baldelli, S.; Campbell, D. J.; Shultz, M. J. *J. Phys. Chem. A* **1999**, *103*, 6383.
(43) Gopalakrishnan, S.; Jungwirth, P.; Tobias, D. J.; Allen, H. C. *J. Phys. Chem.* **2005**, *109*, 8861.
(44) Liu, D.; Ma, G.; Levering, L. M.; Allen, H. C. *J. Phys. Chem. B* **2004**, *108*, 2252.
(45) Johnson, C. M.; Tyrode, E.; Baldelli, S.; Rutland, M. W.; Leygraf, C. *J. Phys. Chem. B* **2005**, *109*, 321.
(46) Tyrode, E.; Johnson, C. M.; Baldelli, S.; Leygraf, C.; Rutland, M. W. *J. Phys. Chem. B* **2005**, *109*, 329.
(47) Buch, V.; Devlin, J. P. *J. Chem. Phys.* **1999**, *110*, 3437.
(48) Brudermann, J.; Melzer, M.; Buck, U.; Kazimirski, J. K.; Sadlej, J.; Buch, V. *J. Chem. Phys.* **1999**, *110*, 10649.
(49) Buck, U.; Ettischer, I.; Melzer, M.; Buch, V.; Sadlej, J. *Phys. Rev. Lett.* **1998**, *80*, 2578.
(50) Devlin, J. P.; Sadlej, J.; Buch, V. *J. Phys. Chem. A* **2001**, *105*, 974.
(51) Pribble, R. N.; Zwier, T. S. *Science* **1994**, *265*, 75.
(52) Steinbach, C.; Andersson, P.; Kazimirski, J. K.; Buck, U. *J. Phys. Chem. A* **2004**, *108*, 6165.
(53) Jungwirth, P.; Tobias, D. J. *J. Phys. Chem. B* **2002**, *106*, 6361.
(54) Scherer, J. R. In *Advances in Infrared and Raman Spectroscopy*; Clark, R. I. H., Hester, R. E., Eds.; Heyden: London, 1978; Vol. 5, p 149.
(55) Scherer, J. R.; Go, M. K.; Kint, S. *J. Phys. Chem.* **1973**, *77*, 2108.
(56) Corcelli, S. A.; Skinner, J. L. *J. Phys. Chem. A* **2005**, *109*, 6154.
(57) Shin, J.-W.; Hammer, N. I.; Diken, E. G.; Johnson, M. A.; Walters, R. S.; Jaeger, T. D.; Duncan, M. A.; Christie, R. A.; Jordan, K. D. *Science* **2004**, *304*, 1137.
(58) Walters, R. S.; Pillai, E. D.; Duncan, M. A. *J. Am. Chem. Soc.* **2005**, *127*, 16599. McCoy, A. B. (private communication).
(59) Buch, V.; Devlin, J. P. *J. Chem. Phys.* **1991**, *94*, 4091.
(60) *The Hydrogen bond: recent developments in theory and experiments*; Schuster, P., Zundel, G., Sandorfy, C., Eds.; North-Holland Pub. Co.: Amsterdam, 1976; Vol. II.
(61) Lilley, T. H. In *Water, A Comprehensive Treatise*; Frank, F., Ed.; New York, 1973; Vol. 3.
(62) Verrall, R. E. In *Water, A Comprehensive Treatise*; Frank, F., Ed.; New York, 1973; Vol. 3.
(63) Jungwirth, P.; Curtis, J. E.; Tobias, D. J. *Chem. Phys. Lett.* **2003**, *367*, 704.
(64) Foster, K. L.; Plastridge, R. A.; Bottenheim, J. W.; Shepson, P. B.; Finlayson-Pitts, B. J.; Spicer, C. W. *Science* **2001**, *291*, 471.
(65) Foster, K. L.; Tolbert, M. A.; George, S. M. *J. Phys. Chem. A* **1997**, *101*, 4979.
(66) Oum, K. W.; Lakin, M. J.; DeHaan, D. O.; Brauers, T.; Finlayson-Pitts, B. J. *Science* **1998**, *279*, 74.
(67) Knipping, E. M.; Lakin, M. J.; Foster, K. L.; Jungwirth, P.; Tobias, D. J.; Gerber, R. B.; Dabdub, D.; Finlayson-Pitts, B. J. *Science* **2000**, *288*, 301.
(68) Hu, J. H.; Shi, Q.; Davidovits, P.; Worsnop, D. R.; Zahniser, M. S.; Kolb, C. E. *J. Phys. Chem.* **1995**, *99*, 8768.
(69) Gibbs, J. W. *The Collected Works of J. W. Gibbs*; Longmans: New York, 1931; Vol. 1.
(70) Walrafen, G. E.; Chu, Y. C. *J. Phys. Chem.* **1995**, *99*, 11225.
(71) Walrafen, G. E.; Yang, W.-H.; Chu, Y. C. *Supercooled Liquids*; American Chemical Society: Washington, DC, 1997; p 287.
(72) Terpstra, P.; Combes, D.; Zwick, A. *J. Chem. Phys.* **1990**, *92*, 65.
(73) Kropman, M. F.; Bakker, H. J. *Chem. Phys. Lett.* **2003**, *370*, 741.
(74) Laenen, R.; Thaller, A. *Chem. Phys. Lett.* **2001**, *349*, 442.
(75) Schnitzer, C.; Baldelli, S.; Shultz, M. J. *J. Phys. Chem. B* **2000**, *104*, 585.
(76) Raymond, E. A.; Richmond, G. L. *J. Phys. Chem. B* **2004**, *108*, 5051.
(77) Jungwirth, P.; Tobias, D. J. *J. Phys. Chem. B* **2001**, *105*, 10468.
(78) Raymond, R. A.; Tarbuck, T. L.; Brown, M. G.; Richmond, G. L. *J. Phys. Chem. B* **2003**, *107*, 546.
(79) Ghosal, S.; Hemminger, J. C.; Bluhm, H.; Mun, B. S.; Hebenstreit, E. L. D.; Ketteler, G.; Ogletree, D. F.; Requejo, F. G.; Salmeron, M. *Science* **2005**, *307*, 563.
(80) Petersen, P. B.; Saykally, R. J. *Chem. Phys. Lett.* **2004**, *397*, 51.
(81) Finlayson-Pitts, B. J.; Pitts, J. N. *Chemistry of the Upper and Lower Troposphere*; Academic Press: New York, 2000.
(82) Kane, S. M.; Caloz, F.; Leu, M. *J. Phys. Chem. A* **2001**, *105*, 6465.
(83) Reid, J. P.; Sayer, R. M. *Chem. Soc. Rev.* **2003**, *32*, 70.
(84) Keene, W. C.; Sander, R.; Pszenny, A. A. P.; Vogt, R.; Crutzen, P. J.; Galloway, J. N. *J. Aerosol Sci.* **1998**, *29*, 339.
(85) Posfai, M.; Anderson, J. R.; Buseck, P. R.; Shattuck, T. W.; Tindale, N. W. *Atmos. Environ.* **1994**, *28*, 1747.
(86) Chelf, J. H.; Martin, S. T. *J. Geophys. Res.*, [*Atmos.*] **2001**, *106*, 1215.
(87) Prenni, A. J.; Wise, M. E.; Brooks, S. D.; Tolbert, M. A. *J. Geophys. Res.*, [*Atmos.*] **2001**, *106*, 3037.
(88) Sander, R.; Lilieveld, J.; Crutzen, P. J. *J. Atmos. Chem.* **1995**, *20*, 89.
(89) Talbot, R. W.; Dibb, J. E.; Loomis, M. B. *Geophys. Res. Lett.* **1998**, *35*, 1367.
(90) Schnitzer, C.; Baldelli, S.; Shultz, M. J. *Chem. Phys. Lett.* **2000**, *313*, 416.
(91) Baldelli, S.; Schnitzer, C.; Campbell, D. J.; Shultz, M. J. *J. Phys. Chem. B* **1999**, *103*, 2789.
(92) Baldelli, S.; Schnitzer, C.; Shultz, M. J. *Chem. Phys. Lett.* **1999**, *302*, 157.
(93) Baldelli, S.; Schnitzer, C.; Shultz, M. J.; Campbell, D. J. *Chem. Phys. Lett.* **1998**, *287*, 143.
(94) Banham, S. F.; Sodeau, J. R.; Horn, A. B.; McCoustra, M.; Chesters, M. A. *J. Vac. Sci. Technol., A* **1996**, *14*, 1620.
(95) Sodeau, J. R.; Horn, A. B.; Banham, S. F.; Koch, T. G. *J. Phys. Chem.* **1995**, *99*, 6258.
(96) Banham, S. F.; Horn, A. B.; Koch, T. G.; Sodeau, J. R. *Faraday Discuss.* **1995**, *100*, 321.
(97) Koch, T. G.; Banham, S. F.; Sodeau, J. R.; Horn, A. B.; McCoustra, M. R. S.; Chesters, M. A. *J. Geophys. Res.* **1997**, *102*, 1513.
(98) Koch, T. G.; Holmes, N. S.; Roddis, T. B.; Sodeau, J. R. *J. Phys. Chem.* **1996**, *100*, 11402.
(99) Horn, A.; Sodeau, J. R.; Roddis, T. B.; Williams, N. A. *J. Phys. Chem. A* **1998**, *102*, 6107.
(100) Rogac, M. B.; Babic, V.; Perger, T. M.; Neueder, R.; Barthel, J. *J. Mol. Liq.* **2005**, *118*, 111.
(101) Heyrovská, R. *Collect. Czech. Chem. Commun.* **1992**, *57*, 2209.
(102) Heyrovská, R. *J. Electrochem. Soc.* **1996**, *143*, 1789.
(103) Heyrovská, R. *J. Electrochem. Soc.* **1997**, *144*, 2380.
(104) Heyrovská, R. *Croat. Chem. Acta* **1996**, *70*, 39.
(105) Heyrovská, R. *Chem. Listy* **1998**, *92*, 157.
(106) Buch, V.; Sadlej, J.; Aytemiz-Uras, N.; Devlin, J. P. *J. Phys. Chem. A* **2002**, *106*, 9374.
(107) Zundel, G. *Adv. Chem. Phys.* **2000**, *111*, 1.
(108) Randles, J. E. B. *Phys. Chem. Liq.* **1977**, *7*, 107.
(109) Washburn, E. W. *International Critical Tables of Numerical Data, Physics, Chemistry, and Technology*; McGraw-Hill: New York, 1928; Vol. 4.
(110) Baldelli, S.; Schnitzer, C.; Shultz, M. J.; Campbell, D. *J. Phys. Chem. B* **1997**, *101*, 10435.
(111) Radüge, C.; Pflumio, V.; Shen, Y. R. *Chem. Phys. Lett.* **1997**, *274*, 140.
(112) Levering, L. M.; Sierra, R.; Allen, H. C. To be submitted.
(113) Petersen, M. K.; Iyengar, S. S.; Day, T. J. F.; Voth, G. A. *J. Phys. Chem. B* **2004**, *108*, 14804.
(114) Salvador, P.; Curtis, J. E.; Tobias, D. J.; Jungwirth, P. *Phys. Chem. Chem. Phys.* **2003**, *5*, 3752.
(115) Yang, X.; Kiran, B.; Wang, X.-B.; Wang, L.-S.; Mucha, M.; Jungwirth, P. *J. Phys. Chem. A* **2004**, *108*, 7820.
(116) Gurau, M. C.; Kim, G.; Lim, S.-M.; Albertorio, F.; Fleisher, H. C.; Cremer, P. S. *ChemPhysChem* **2003**, *4*, 1231.
(117) Baldelli, S.; Schnitzer, C.; Shultz, M. J. *J. Chem. Phys.* **1998**, *108*, 9817.
(118) Kroes, G.-J.; Clary, D. *J. Phys. Chem.* **1992**, *96*, 7079.
(119) Smart, R. S. C.; Sheppard, N. *J. Chem. Soc., Faraday Trans. 2* **1976**, *72*, 707.
(120) Svanberg, M.; Pettersson, J. B. C.; Bolton, K. *J. Phys. Chem. A* **2000**, *104*, 5787.
(121) Kolb, C. E.; Worsnop, D. R.; Zahniser, M. S.; Davidovits, P.; Keyser, L. F.; Leu, M. T.; Molina, M. J.; Hanson, D. R.; Ravishankara, A. R. In *Advanced Series in Physical Chemistry, Vol. 3: Progress and Problems in Atmospheric Chemistry*; Barker, J., Ed.; World Scientific: Singapore, 1995; p 771.
(122) Watson, L. R.; VanDoren, J. M.; Davidovits, P.; Worsnop, D. R.; Zahniser, M. S.; Kolb, C. E. *J. Geophys. Res.* **1990**, *95*, 5631.
(123) Delzeit, L.; Rowland, B.; Devlin, P. *J. Phys. Chem.* **1993**, *97*, 10312.
(124) Jungwirth, P. *J. Phys. Chem. A* **2000**, *104*, 145.

(125) Jungwirth, P.; Tobias, D. J. *J. Phys. Chem. B* **2000**, *104*, 7702.
(126) Kuo, J.-L.; Klein, M. L. *J. Chem. Phys.* **2005**, *122*, 024516.
(127) James, T.; Wales, D. J. *J. Chem. Phys.* **2005**, *122*, 134306.
(128) Day, T. J. F.; Soudackov, A. V.; Uma, M.; Schmitt, U. W.; Voth, G. A. *J. Chem. Phys.* **2002**, *117*, 5839.
(129) Iyengar, S. S.; Day, T. J. F.; Voth, G. A. *J. Mass. Spectrom.* **2005**, *241*, 197.
(130) Renard, J. J.; Calidonna, S. E.; Henley, M. V. *J. Haz. Mater*. **2004**, *B108*, 29.
(131) Rice, O. K. *J. Phys. Chem.* **1928**, *32*, 583.
(132) Simonelli, D.; Baldelli, S.; Shultz, M. J. *Chem. Phys. Lett.* **1998**, *298*, 400.
(133) Simonelli, D.; Shultz, M. J. *J. Chem. Phys.* **2000**, *112*, 6804.
(134) Shi, Q.; Davidovits, P.; Jayne, J. T.; Worsnop, D. R.; Kolb, C. E. *J. Phys. Chem. A* **1999**, *103*, 8812.
(135) Swartz, E.; Shi, Q.; Davidovits, P.; Jayne, J. T.; Worsnop, D. R.; Kolb, C. E. *J. Phys. Chem. A* **1999**, *103*, 8824.
(136) Baldelli, S.; Schnitzer, C.; Shultz, M. J.; Campbell, D. *J. Phys. Chem. B* **1997**, *101*, 4607.
(137) Donaldson, D. J. *J. Phys. Chem. A* **1999**, *103*, 62.
(138) Davidovits, P.; Hu, J. H.; Worsnop, D. R.; Zahniser, M. S.; Kolb, C. E. *Faraday Discuss.* **1995**, *100*, 65.
(139) Reid, J. P.; Sayer, R. M. *Chem. Soc. Rev.* **2002**, *32*, 70.
(140) Dang, L. X.; Garrett, B. C. *Chem. Phys. Lett.* **2004**, *385*, 309.
(141) Bacelo, D. E. *J. Phys. Chem. A* **2002**, *106*, 11190.
(142) Buck, U.; Huisken, F. *Chem. Rev.* **2000**, *100*, 3863.
(143) Devlin, J. P.; Joyce, C.; Buch, V. *J. Phys. Chem. A* **2000**, *104*, 1974.
(144) Xantheas, S. S. *Chem. Phys.* **2000**, *258*, 225.
(145) *Water in Confining Geometries*; Springer-Verlag: Amsterdam, 2003.
(146) Danten, Y.; Tassaing, T.; Besard, M. *J. Phys. Chem. A* **2000**, *104*, 9415.
(147) Köddermann, T.; Schulte, F.; Huelsekopf, M.; Ludwig, R. *Angew. Chem., Int. Ed.* **2003**, *42*, 4904.
(148) Magnusson, L. B. *J. Phys. Chem.* **1970**, *74*, 4221.
(149) Kuo, M.; Shultz, M. J. To be submitted.
(150) Rowland, B.; Kadagathur, N. S.; Devlin, J. P.; Buch, V.; Feldman, T.; Wojcik, M. J. *J. Chem. Phys.* **1995**, *102*, 8328.

CR040361N